Stability and
Controllability of a Formula One Racing Car

by

Alexander Haslam (EM)

Fourth Year Undergraduate Project

in Group C, 2011/2012

I hereby declare
that, except where specifically indicated, the work submitted herein is my own original work.

Signed: ..... *Date: 30/05/2012*

Stability and Controllability of a Formula One Racing Car

by

Alexander Haslam (EM)

Fourth Year Undergraduate Project
in Group C, 2011/2012

Abstract

In the Formula One (F1) industry, despite the numerous technological advances, there is a still a need for a more efficient method for objectively characterising vehicle handling behaviour. Such a metric would have to be able to deal with the highly non-linear and transient behaviour of the vehicle at the limits of tyre adhesion. This project aimed to develop metrics to fulfill these criteria.

There are many rigorous methods for characterising stability and controllability, both analytical from control theory and vehicle dynamics, as well as more experimental based methods, but the majority of these are not feasible for the F1 industry. Previous work on vehicle stability suggested the use of state variances as a potential solution to this problem, and this project aims to develop this concept further.

A 5 degree-of-freedom vehicle model was created, with variable longitudinal speed and a non-linear tyre model A neuromuscular filter was included between the driver's commanded steering angle, and the true steering wheel angle, to model the dynamics of the driver's arms, and a Linear-Quadratic Controller was added to model the closed-loop control from the driver. As a comparison, stability derivatives were also computed along the vehicle trajectory, which are already used by some F1 teams. These essentially give the damping coefficient and torsional spring which govern the yaw motion of the vehicle.

The stability was investigated first. The standard deviations of the vehicle states, due to pre-specified disturbances, were computed as a function of time during a manoeuvre. Both steering disturbances from the driver, as well as as lateral force and yaw moment disturbances, were included. The closed-loop control from the driver was essential to ensure that the standard deviations of the vehicle states would settle towards zero again after a manoeuvre, as expected, which was not the case in the previous work. The stability derivatives were also computed. The key advantage of these methods, was that they could all be computed in real-time with the vehicle simulation, and iterations were not required. From a short sample manoeuvre, it was concluded that the state variance method

could give results which are easier to interpret. This is because one value, such as the standard deviation of the lateral path error could be quoted, to give a quantitative impression of the stability. On the other hand, the interaction between the two stability derivatives made them more ambiguous, and the yaw stiffness was often negative, whilst the vehicle is still observed to be practically stable.

These ideas were then extended to controllability. The standard deviation of the driver's control inputs could be computed, in a similar manner to the state standard deviations. Similarly, controllability derivatives, were calculated. These are essentially "stiffness" terms which depict the change in the lateral force and moment generated from a small increment in steering angle. Thus, in each case, the driver's steering effort could be measured, and hence the lateral controllability characterised. Again, from a short sample manoeuvre, it was concluded that the variance-based method could give results which are easier to interpret, compared to the controllability derivatives.

The main use of such metrics would be to guide set-up changes for the vehicle, so a parameter study was carried out. This consisted of firstly, using an existing program to find the control inputs required to guide the vehicle along an optimal trajectory, around a 90° bend. These controls could then be fed into the existing vehicle model and stability and controllability metrics, to find both the vehicle trajectory and resulting handling behaviour. The manoeuvre time was also recorded, to give a measure of performance. This process was carried out first for the nominal vehicle set-up, and then for variations from this, with only one parameter being varied at a time. Thus, the effect of each parameter; namely the brake balance, centre of gravity, wheelbase, yaw moment of inertia, as well as the fraction of the friction circle used; was isolated. Additionally, this allowed the relative metrics to be assessed further. However, it was found that, in this case, although the variance-based metrics generally gave more succinct and easy to interpret measures of the stability and controllability, the derivatives were found to provide a better insight into the mechanics of the vehicle. They are therefore perhaps more useful when trying to suggest beneficial set-up changes.

In conclusion, it was deemed that the aim of the project, was fulfilled. Both the variance-based metrics and derivatives characterised the stability and controllability, and were computationally efficient to compute. They also dealt well with the high degree of non-linearity in the system. Although the variance-based methods were deemed to produce simpler to understand metrics, the derivatives gave better insight into the mechanics of the vehicle, and so are particularly important when trying to optimise the set-up. Therefore, the recommendation was that a combination of both types of metric could of most benefit. However, these metrics would require further development, before they could be implemented in a practical setting; a more rigorous parameter study may be of interest and reveal more complex trends. More accurate vehicle and driver models may also be required, to reflect the handling behaviour accurately, for which the computational efficiency has yet to be investigated, and ways to characterise the longitudinal stability have yet to be found. Nevertheless, there is evidence to suggest that these metrics are very promising, and have potentially far-reaching applications.

Contents

List of Figures **3**

List of Tables **3**

Nomenclature **4**

Acknowledgements **5**

1 Introduction & Aim **6**

2 Literature Review & Objectives **6**

2.1 Control Theory 7

2.2 Vehicle Dynamics 7

2.3 Previous Work 8

2.4 Objectives 9

3 Vehicle Model **10**

3.1 Equations of Motion 10

3.2 Lateral Path Error 11

3.3 Position 12

3.4 Tyre Model 13

3.5 Driver Neuromuscular System (NMS) 15

3.6 Disturbances 16

3.7 State-Space Model 17

4 Driver Model **18**

4.1 Linear Quadratic Control 18

4.2 Weighting Matrices 19

4.3 Results 20

4.4 Bandwidth and Delays 21

5 Stability Metrics **22**

5.1 Stability Derivatives 22

5.2 State Variance Matrices 23

5.3 Comparison 24

6 Controllability Metrics **25**
6.1 Controllability Derivatives . . . 25
6.2 Control Variance Matrix . . . 26
6.3 Comparison . . . 27

7 Parameter Study **28**
7.1 Methodology . . . 28
7.2 Track Geometry . . . 28
7.3 Computation of Optimal Vehicle Trajectories . . . 29
7.4 Results for the Nominal Vehicle Parameters . . . 29
7.5 Results with Varying Vehicle Parameters . . . 32
7.5.1 Brake Balance . . . 33
7.5.2 Centre of Gravity Position . . . 35
7.5.3 Moment of Inertia . . . 37
7.5.4 Wheelbase . . . 39
7.5.5 Tyre Slip Limit . . . 41

8 Conclusions **43**

9 Future Work **45**

Risk Assessment Retrospective **46**

References **47**

List of Figures

1 State-space trajectories for vehicle with a zero steer input at $30\,\mathrm{ms}^{-1}$ 7
2 Correlation between steering wheel angle, and yaw rate and lateral acceleration for an ISO lane change for a road vehicle 8
3 Lateral, longitudinal and yaw dynamics of 5 DOF bicycle model 10
4 Lateral Path Error 12
5 Kinematics of the vehicle position 13
6 "Magic tyre formula" force characteristics 15
7 Time histories of lateral velocity and accelerations due to external disturbances with large superelevation and strong winds 16
8 Simulation of a left-handed turn at $30\,\mathrm{ms}^{-1}$ 21
9 Power spectral density of the driver controls for a left-handed turn at $30\,\mathrm{ms}^{-1}$ 22
10 Definition of stability derivatives 22
11 Ensembled state standard deviations of a left-handed turn at $30\,\mathrm{ms}^{-1}$ 24
12 Stability metrics for a left-handed turn at $30\,\mathrm{ms}^{-1}$ 25
13 Ensembled control input standard deviations of a left-handed turn at $30\,\mathrm{ms}^{-1}$ 26
14 Controllability metrics for a left-handed turn at $30\,\mathrm{ms}^{-1}$ 28
15 Flow chart of parameter study 29
16 Track geometry used for the parameter study 29
17 Stability and controllability metrics for the nominal vehicle setup on an optimal trajectory around a 90° bend 30
18 Variation of stability with brake balance 33
19 Variation of controllability with brake balance 34
20 Variation of performance with brake balance 34
21 Variation of stability with centre of gravity position 36
22 Variation of controllability with centre of gravity position 37
23 Variation of performance with centre of gravity position 37
24 Variation of stability with yaw moment of inertia 38
25 Variation of controllability with yaw moment of inertia 39
26 Variation of performance with yaw moment of inertia 39
27 Variation of stability with wheelbase 40
28 Variation of controllability with wheelbase 41
29 Variation of performance with wheelbase 41
30 Variation of stability with tyre slip limit 42
31 Variation of controllability with tyre slip limit 43
32 Variation of stability, controllability and performance with tyre slip limit 43

List of Tables

1 Vehicle parameters 11
2 Tyre parameters 14
3 Driver NMS parameters 15
4 Statistics of disturbances 17
5 LQR weighting matrices elements 20

Nomenclature

$\mathbf{A}_c, \mathbf{B}_c, \mathbf{H}_c, \mathbf{F}_c$	Continous-Time State-Space Matricies
$\mathbf{A}_k, \mathbf{B}_k, \mathbf{H}_k, \mathbf{F}_k$	Discrete-Time State-Space Matricies
α_f, α_r	Lateral Slip of Front/Rear Tyres
B, C, D, E	Magic Tyre Formula Coefficients
b_f	Brake Balance to Front
c_1, c_2	Cornering Stiffness Paramaters
C_α	Lateral and Longitunal Slip Stiffness
C_f, C_r	Linear Lateral Tyre Constant of Front/Rear Axle
δ	Steering Angle
δ_{com}	Commanded steering wheel angle
δ_{dist}	Steering disturbance
Δu_k	Perturbation of u from the nominal input
Δw_k	Perturbation of w from the nominal case
Δx_k	Perturbation of x from the nominal state
δ_{sw}	Steering Wheel Angle
e	Lateral Path Error
F_p	Friction Circle Radius
$F_{x,f}, F_{x,r}$	Longitudinal Load on Front/Rear Axle
F_y	Total Lateral Force on Vehicle
$F_{y,dist}$	Lateral Disturbance on Vehicle
$F_{y,f}, F_{y,r}$	Lateral Load on Front/Rear Axle
F_z	Vertical Load on Vehicle
$F_{z,f}, F_{z,r}$	Vertical Load on Front/Rear Axle
g	Acceleration due to Gravity
G_{sw}	Steering Gain
I_f, Ir	Moment of Inertia of Front/Rear Wheels
I_z	Vehicle Yaw Moment of Inertia
$\mathbf{K}_k$	Discrete-Time State Feedback Gain Matrix
κ_f, κ_r	Longitudinal Slip of Front/Rear Tyres
L	Wheelbase
l_f, l_r	Distance from CoG to Front/Rear Axle
m	Vehicle Mass
M_z	Total Yaw Moment on Vehicle
$M_{z,dist}$	Yaw Disturbance on Vehicle
ω_f, ω_r	Front/Rear Axle Angular Velocity

ω_n	Natural Frequency of NMS System
ψ	Yaw Angle
$\mathbf{Q}, \mathbf{R}$	Cost Function Weighting Matricies
r_f, r_r	Radius of Front/Rear Wheels
ρ	Local Radius of Curvature of Track
θ	Local Attitude of Track in Global Reference Frame
$\underline{s}$	Normalised Slip Vector
s	Distance Along Track Centreline
$\sigma_{\delta_{dist}}$	Standard Deviation of Steering Disturance
$\sigma_{F_{y,dist}}$	Standard Deviation of Lateral Force Disturance
$\sigma_{M_{z,dist}}$	Standard Deviation of Yaw Moment Disturance
S_V, S_H	Vertical/Horiztonal Shift in Magic Tyre Formula
T	Drive/Brake Torque demanded by Driver
t	Distance from Track Centreline
T_f, Tr	Torque acting on Front/Rear Axle
u	Control Input Vector
$\bar{u}_k$	Nominal Control Input Vector
V_x	Longitudinal Velocity
V_y	Lateral Velocity
w	Disturbance Vector
$\bar{w}_k$	Nominal Disturbance Vector
X	X co-ordinate of Vehicle in Global Reference Frame
x	State Vector
x_0, u_0, w_0	Linearisation Point
$\bar{x}_k$	Nominal State Vector
Y	Y Co-ordinate in Global Reference Frame
y	Lateral Path Error Generating State
ζ_n	Damping Factor of NMS System

Acknowledgments

The author would like to thank Dr David Cole for his help and advice throughout the project. Two of the main software tools used in the project, the symbolic solver in section 3.7 and the optimal path finder tool in section 7, were provided by Julian Timings. Particular thanks goes to him, both for his willingness to hand over the products of his PhD thesis, but also for the ongoing technical support for them which he provided.

1 Introduction & Aim

Formula One (F1) is a long-running single seat racing championship in which 12 teams compete, each entering two cars, and is seen as the pinnacle of motorsport and automotive engineering in general. The Fédération Internationale de l'Automobile (FIA) and Formula One Teams Association (FOTA) together agree a set of rules, which are known as a "formula" to which all of the competitors must conform to. A wide variety of parameters as well as technologies are fixed, and there are also limitations on the resources used, in an effort to keep the sport more competitive and in keeping with the current economic situation. All cars now use the same Pirelli tyres, so as to ensure reliability and to reduce development costs for the teams.

All of the teams put a great deal of effort into making the best use of their resources, in order to optimise the design of the car. Many aspects including the aerodynamics of the vehicle can be aided using computational methods, but this can be particularly effective for race strategy as well as vehicle dynamics, which is the area of interest for this work. They are able to simulate various laps of the vehicle for each set-up, with a highly sophisticated model. The effect on performance can be easily determined from metrics such as lap times and fuel consumption, allowing an initial "optimum" to be found. However, the handling behaviour is just as important, so as to ensure that driver can unlock the full performance of the vehicle. This is much more difficult to objectively measure, so there is therefore a greater reliance on "rules of thumb" during design as well as driver feedback.

It is the intention of this project to provide a potential solution to this problem, by developing a method which can give a quantitative depiction of the vehicle behaviour, so that an improved initial "optimum" can be found. Specifically, the aim of this project is to develop a metric for characterising the stability and controllability of an F1 car, whilst at the limits of tyre adhesion and at high speed. This would allow the effect of set-up changes on handling to be objectively predicted. Such a method must be computationally efficient, and also ideally in real time with the simulation, maximising the number of simulations which can be run. The method must also be able to handle the high-degree of non-linearities in the system, most significantly from the tyres, which complicates the modeling process.

2 Literature Review & Objectives

At the beginning of this project, the work of various researchers from a variety of fields was examined, in order to assess the applicability of existing metrics and methodologies. Of particular interest was the work of Sideris [1], who carried out a detailed investigation into four potential stability metrics specifiable applicable to F1, from which this work follows directly.

2.1 Control Theory

There are already numerous ways to characterise the stability of both linear and non-linear systems from the field of control theory. Many studies including [2] plot state-space trajectories, which are essentially vector fields, which graphically depict the time-domain response. An example is shown in figure 1. This model used in this work had only 2 degrees of freedom, so the trajectories are planar, but in general, they will be in a multi-dimensional space.

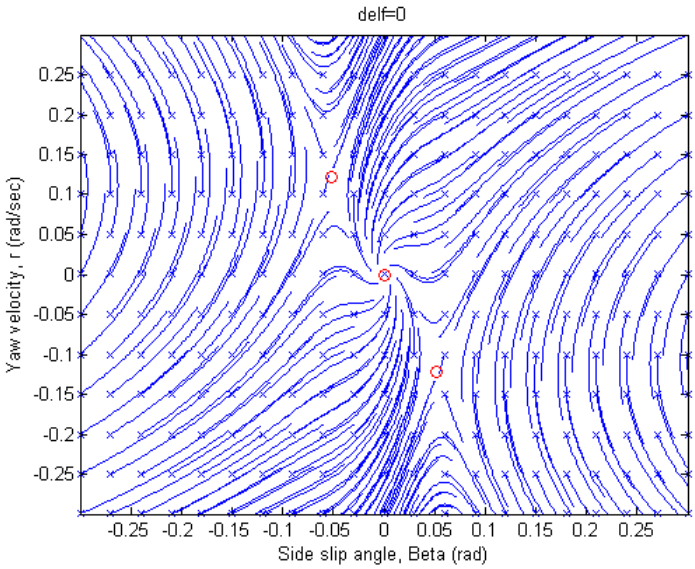


Figure 1: State-space trajectories for vehicle with a zero steer input at $30\,\mathrm{ms}^{-1}$ [2]

If the vehicle is stable, the trajectories will converge to a minimum which will be an equilibrium point, such as the origin in figure 1 marked with a red circle; this is a stable spiral. However, if there is saddle point or a maximum, the vehicle will drift away from this point, and the other two red circles in figure 1 are examples of this. This gives a definite clarification of stability, but numerous computations are required in order to simply generate a plot, and the complexity dramatically increases once more degrees of freedom are added to the model, so are not applicable for this work.

2.2 Vehicle Dynamics

Sideris [1] carried out an extensive review of the various measures of stability in the field of vehicle dynamics. Many studies only look at manoeuvres at constant speed, and often steady-state conditions, as this greatly simplifies the analysis. Pacjeka for example in [3], produced handling diagrams from such studies, which give the required steady-state steer angle as a function of lateral acceleration, which allows the definition of understeer and oversteer behaviour. Other studies assumed simpler models, with linear tyres, which allow other definitions of handling behaviour, such as the static margin, which is the distance aft of the centre of gravity (CoG) where the net tyre force can be considered to act on a linear vehicle, as a proportion of the wheelbase. If it is positive, then the vehicle is

understeering and vice versa [4]. The main limitation of these methods is that they are cannot account for the transient behaviour of an F1 car, which have a highly variable forward speed. Also, there is little consideration of the controllability in these studies, since open-loop motion is usually assumed.

Others such as Kohn [5] have looked at more experimental methods. Various standard tests were run on instrumented cars, and correlations and time delays between the input and output parameters were found, giving an indication of the predictability in the behaviour. For example, in figure 2, the correlation between the lateral acceleration and the steering wheel angle reduces with increasing speed (marked with squares), for a vehicle completing a standardised lane change manoeuvre. This indicates that the behaviour is less predictable, so it is more difficult for the driver to control the vehicle. Electronic stability systems assess the stability of the vehicle, by measuring the difference in the response of the real vehicle to that of a simple linear vehicle. When this difference exceeds a threshold, the system intervenes. However, there are various ways to choose a suitable threshold [1]. The issue with these methods is that prototypes and much testing are required, which would be extremely costly for the F1 industry and are therefore not practical.

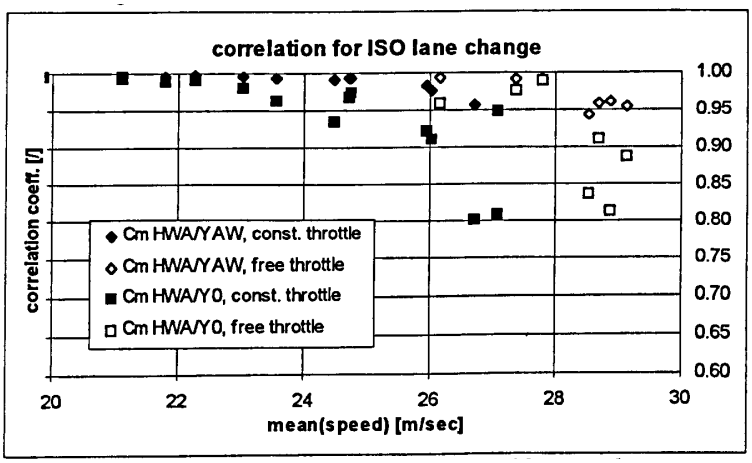


Figure 2: Correlation between steering wheel angle, and yaw rate and lateral acceleration for an ISO lane change for a road vehicle [5]

2.3 Previous Work

Sideris [1] after his literature review began a detailed investigation into four methods of characterising stability, specifiable applicable to F1 cars. This project follows on directly from his work. Firstly, the open loop eigenvalues of the system were analysed for each time step during manoeuvres. These eigenvalues are analogous to the poles of transfer functions, so the eigenvalues must have a negative real part for the system to be stable. However, this analysis was not strictly valid as it requires the system to be approximately time-invariant so near equilibrium [6], whereas this is rarely the car for an F1 car.

Stability derivatives [4] are a measure which is currently used by some F1 teams to assess handling performance from measured or simulated data. This consists of finding the stiffness k and viscosity

λ of a virtual torsional spring and damper connected to the car, which govern the yaw dynamics. From the Routh-Hurwitz stability criterion, it is required that both of these derivatives, k and λ, are positive for the system to be classified as stable [7]. This method gave some insightful predictions, but the results were somewhat difficult to interpret in certain cases, because in realty the situation is more complex so the Routh-Hurwitz criterion do not apply.

The Practical Stability Index (PSI) was then investigated by Sideris. The weighted total of the perturbations of the vehicle states over time, due to uncertainties in the initial conditions, is computed, and then compared to a pre-specified acceptable range of values. From this, the largest signular value of a matrix (which is known as the PSI) can be computed, which gives a measure of how close the real states are to the limit. If this exceeds unity, then the system can be classified as unstable, and vice versa [8]. However, it was difficult to decide upon suitable limits. Therefore, this idea was extended to computing the variance of the vehicle states due to pre-specified Gaussian disturbances. This was very efficient to compute, and it gives tangible real-world values for the stability. However, the variance of the lateral path error remained unbounded in Sideris' study, which was later found to be because there was no driver in the loop to recentre the car. It was concluded that this method had the greatest potential if these issues could be fixed.

2.4 Objectives

It was decided that in order to achieve the overall aim, this project would focus on solving the problems with the state variance method in [1], with stability derivatives used as a comparison, but then also extend these ideas to controllability. Additionally, with these new metrics, it would be useful to then draw some conclusions regarding the mechanics of the vehicle set-up. The following five major objectives are therefore to this end.

1. A closed-loop controller must be implemented to model the driver in the loop, to ensure all of the state variances remain bounded.

2. Extend the state variance and stability derivative methods to find analogous metrics for determining the controllability.

3. Be able to find optimal trajectories of the vehicle round specific bends, which will be achieved using existing software.

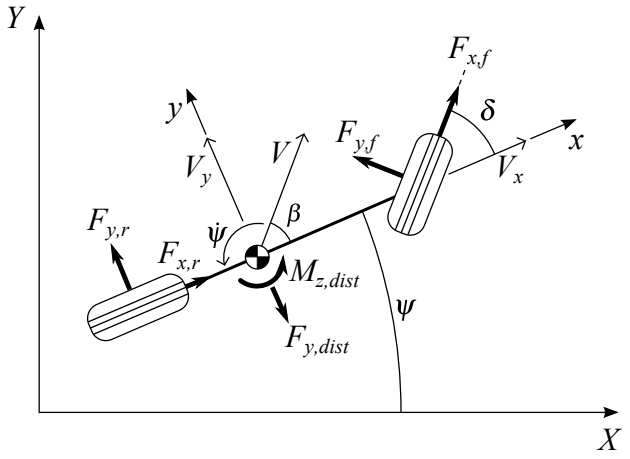
4. Assess the stability and controllability of the vehicle by computing the various metrics along these trajectories, and compare their merits.

5. Carry out a parameter study, to examine the effects of setup changes on vehicle handling, which is the main use of such metrics.

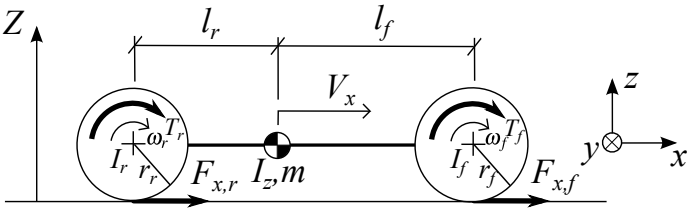
3 Vehicle Model

3.1 Equations of Motion

In order to give a realistic prediction of the dynamic behaviour of the vehicle, a simple 5 degree of freedom "bicycle" model was created in MATLAB. This assumes that the two front wheels are each "averaged" together, so as to create a two wheeled vehicle as shown in figure 3.



(a) Plan view



(b) Side elevation

Figure 3: Lateral, longitudinal and yaw dynamics of 5 DOF bicycle model

The degrees of freedom are the yaw rate $\dot{\psi}$, lateral velocity V_y and longitudinal velocity V_x, as well as the angular velocities of each of the front and rear wheels ω_f and ω_r. The five equations of motion can be expressed as follows [9]:

$$\dot{V}_y = \frac{1}{m}\left(F_{y,f}\cos\delta + F_{x,f}\sin\delta + F_{y,r} + F_{y,dist}\right) - V_x\dot{\psi} \tag{3.1.1}$$

$$\dot{V}_x = \frac{1}{m}\left(-F_{y,f}\sin\delta + F_{x,f}\cos\delta + F_{x,r}\right) + V_y\dot{\psi} \tag{3.1.2}$$

$$\ddot{\psi} = \frac{1}{I_z}\left(F_{y,f}l_f\cos\delta + F_{x,f}l_f\sin\delta + F_{y,r}l_r + M_{z,dist}\right) \tag{3.1.3}$$

$$\dot{\omega}_f = \frac{1}{I_f}\left(T_f - F_{x,f}r_f\right) \tag{3.1.4}$$

$$\dot{\omega}_r = \frac{1}{I_r}\left(T_r - F_{x,r} r_r\right) \tag{3.1.5}$$

The disturbance terms $F_{y,dist}$ and $M_{z,dist}$ have been included and will be described later in section 3.6 on page 16. The front and rear axle torques T_f and T_r are yet to be defined. However, noting that the drive/brake torque T specified by the driver will be split between the front and rear axles according to the front brake balance b_f under braking, but during acceleration, all of the torque travels to the rear axle, assuming a rear wheel driven vehicle, suitable definitions are [9]:

$$T_f = b_f\left(1 - H(T)\right)T \tag{3.1.6}$$

$$T_r = T - T_f \tag{3.1.7}$$

where the function $H(z)$ is the Heaviside step function.

The parameters used for the vehicle model in this project are listed in table 1. They are representative of a typical four-door road car, and are therefore in no way representative of an F1 car, but it is nevertheless enough to assess the merits of the various stability and controllability metrics.

Parameter	Symbol	Value
Mass	m	1050 kg
Moment of Inertia about Z axis	Iz	1500 kg m^2
Front axle to CoG distance	l_f	1.38 m
Rear axle to CoG distance	l_r	0.92 m
Front Wheel Radius	r_f	0.28 m
Rear Wheel Radius	r_r	0.28 m
Front axle Moment of Inertia	I_f	2.00 m
Rear axle Moment of Inertia	I_r	2.00 m
Front Brake Balance	b_f	0.45

Table 1: Vehicle parameters

3.2 Lateral Path Error

The linear-quadratic controller in section 4 on page 18 will require an expression for the lateral error from the nominal path, due to perturbations in the vehicle states. Letting the perturbed lateral and longitudinal velocities be $V_y + \Delta V_y$ and $V_x + \Delta V_x$ respectively, and the perturbed yaw angle be $\psi + \Delta\psi$, and looking at figure 4 on the following page above, it can be noted that (neglecting second order terms):

$$\begin{aligned} \dot{e} &= (V_y + \Delta V_y) + (V_x + \Delta V_x)\Delta\psi - V_y \\ &= \Delta V_y + V_x \Delta\psi \end{aligned} \tag{3.2.1}$$

where $\Delta\psi$ has been assumed small. In order to be able to generate this equation later in the perturbation equation (4.1.1), the addition of the following state (see section 3.7 on page 17) was considered [10]:

$$\dot{y} = V_y + V_x\psi \tag{3.2.2}$$

For the nominal case with large angles ψ, this is a meaningless equation. However, when small perturbations are considered later about a linearisation point y_0, as in equation (4.1.1), this reduces

to the expression below:

$$\begin{aligned}\dot{y}_0 + \Delta\dot{y} &= \left(V_{y,0} + \Delta V_y\right) + \left(V_{x,0} + \Delta V_x\right)\left(\psi_0 + \Delta\psi\right) \\ &= \left(V_{y,0} + V_{x,0}\psi_0\right) + \left(\Delta V_y + V_{x,0}\Delta\psi + \psi_0 \Delta V_x\right) \\ \Leftrightarrow \Delta\dot{y} &= \Delta V_y + V_{x,0}\Delta\psi + \psi_0 \Delta V_x \end{aligned} \tag{3.2.3}$$

because $\dot{y}_0 = \left(V_{y,0} + V_{x,0}\psi_0\right)$. If $\Delta y \triangleq e$, looking at equations (3.2.1) and (3.2.3), it is clear the linearisation point must always be taken about $V_{x,0} = V_x$, the current nominal longitudinal velocity. However, it must be linearised about $\psi_0 = 0$, rather than the true current yaw angle, which ensures that the lateral path error is independent on the heading in the global XY reference frame as expected. This shifting of the ψ linearisation point does not reduce the accuracy of the other state equations late in section 3.1, since none of them involve ψ, only its derivatives.

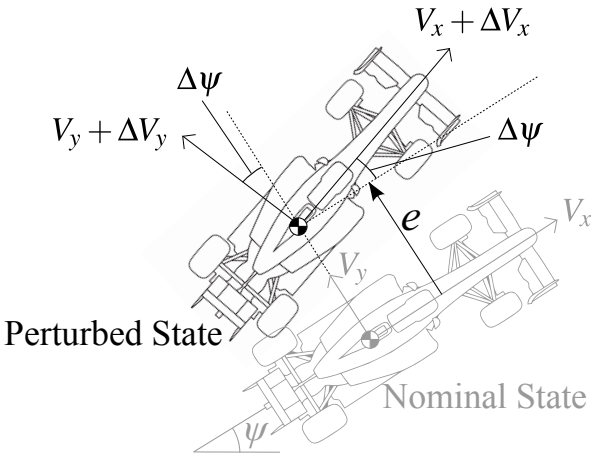


Figure 4: Lateral Path Error

3.3 Position

It was necessary to also be able to calculate the position of the vehicle, both a fixed Cartesian frame, and in intrinsic co-ordinates aligned with the track centre line. The lateral track displacement can can be computed from the following differential equation:

$$\dot{t} = V_x \cdot (\psi - \theta) + V_y \tag{3.3.1}$$

where θ is the attitude of the track at the current position. This is only valid for small $(\psi - \theta)$, so when the vehicle is nearly parallel to the road, but this is a reasonable assumption. Similarly, the distance along the track centre-line can be found:

$$\dot{s} = \frac{\rho}{\rho - t}\left(V_x - V_y \cdot (\psi - \theta)\right) \tag{3.3.2}$$

where ρ is the radius of curvature at the current position.

The position in the global X,Y co-ordinate system can be found by integrating the differential equations:

$$\dot{X} = V_x \cos\psi - V_y \sin\psi \tag{3.3.3}$$

$$\dot{Y} = V_x \sin\psi + V_y \cos\psi \tag{3.3.4}$$

These co-ordinates are defined in figure 5 on the facing page.

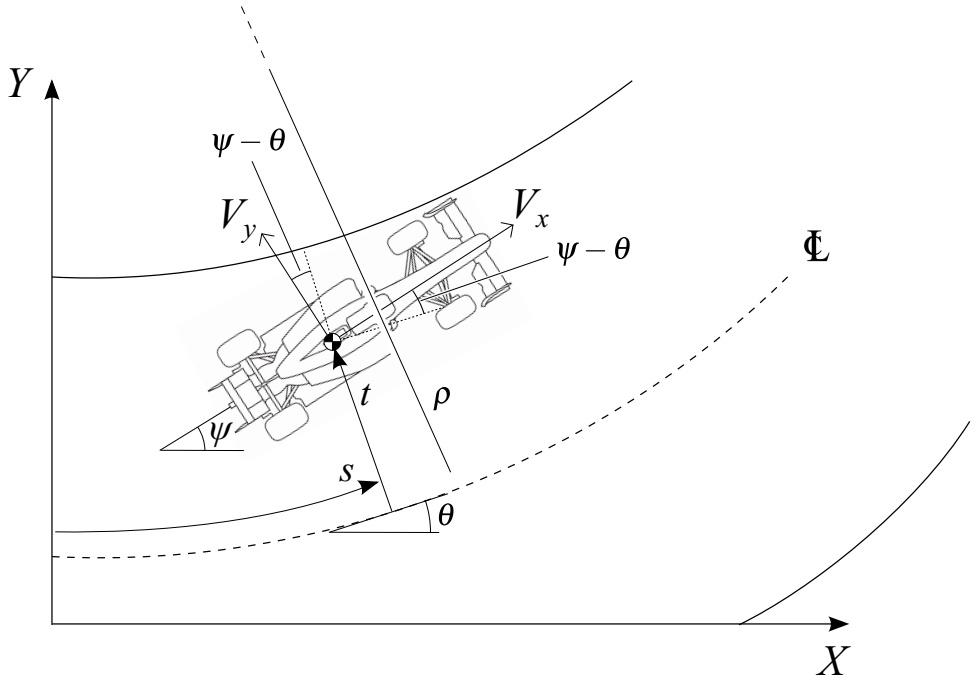


Figure 5: Kinematics of the vehicle position

3.4 Tyre Model

The tyre forces can in turn be expressed as functions of the lateral and longitudinal slips. These are defined as follows:

$$\alpha_f \triangleq \delta - \frac{V_y + \dot{\psi} l_f}{V_x} \qquad (3.4.1) \qquad \alpha_r \triangleq -\frac{V_y - \dot{\psi} l_r}{V_x} \qquad (3.4.2)$$

$$\kappa_f \triangleq \frac{\omega_f r_f - V_x}{|V_x|} \qquad (3.4.3) \qquad \kappa_r \triangleq \frac{\omega_r r_r - V_x}{|V_x|} \qquad (3.4.4)$$

The tyre forces will be linear functions of these slips in the case of small slip so that $F_{y,f} = C_f \alpha_f$ and $F_{x,f} = C_f \kappa_f$ etc., but for larger slips, as is the case for an F1 car at the limits of adhesion, the tyre force approaches the frictional limit. In the case of combined slips, since it is the combined tyre force $F = \sqrt{F_x^2 + F_y^2}$ which is limited by friction, the situation is more complex and the friction limit in the slip plane is circular. To model these effects, the normalised combined slip are introduced [9, 11]:

$$\underline{s} = \begin{bmatrix} s_x \\ s_y \end{bmatrix} = \frac{C_\alpha}{F_p} \begin{bmatrix} \tan\alpha \\ \kappa \end{bmatrix} \qquad (3.4.5)$$

where α and κ are the lateral and longitudinal slips for the wheel in question. F_p is the radius of the friction circle and is given by [9, 11]:

$$F_p = \frac{F_z}{1 + \left(\frac{3F_z}{2mg}\right)^3} \qquad (3.4.6)$$

F_z is the vertical load on the tyre. it can be noted that F_p is an increasing function of F_z which models the increase of the total friction force available with increased vertical load. This effect does

eventually peak off as the tyres saturate, which is achieved by denominator in equation (3.4.6). In this work, weight transfers due to longitudinal acceleration and roll and heave dynamics, and aerodynamic down-force terms were neglected for simplicity so that only the static force from the vehicle weight is left. That is:

$$F_{z,f} = \frac{l_r}{L} mg \qquad (3.4.7) \qquad\qquad F_{z,r} = \frac{l_f}{L} mg \qquad (3.4.8)$$

where the wheelbase L has been introduced with $L = l_r + l_f$. Looking back at equation (3.4.5), C_α is the lateral and longitudinal slip stiffness and is given by the equation [9, 11]:

$$C_\alpha = c_1 \left(1 - \exp\left(-\frac{F_z}{c_2} \right) \right) \qquad (3.4.9)$$

This eventually allow the tyre forces to be computed as follows [9, 11]:

$$\begin{bmatrix} F_x \\ F_y \end{bmatrix} = P(z) \frac{F_p}{|\underline{s}|} \begin{bmatrix} s_x \\ s_y \end{bmatrix} \qquad (3.4.10)$$

where the function $P(z)$ is the known as the "Magic Tyre Formula" [12] and is of the form:

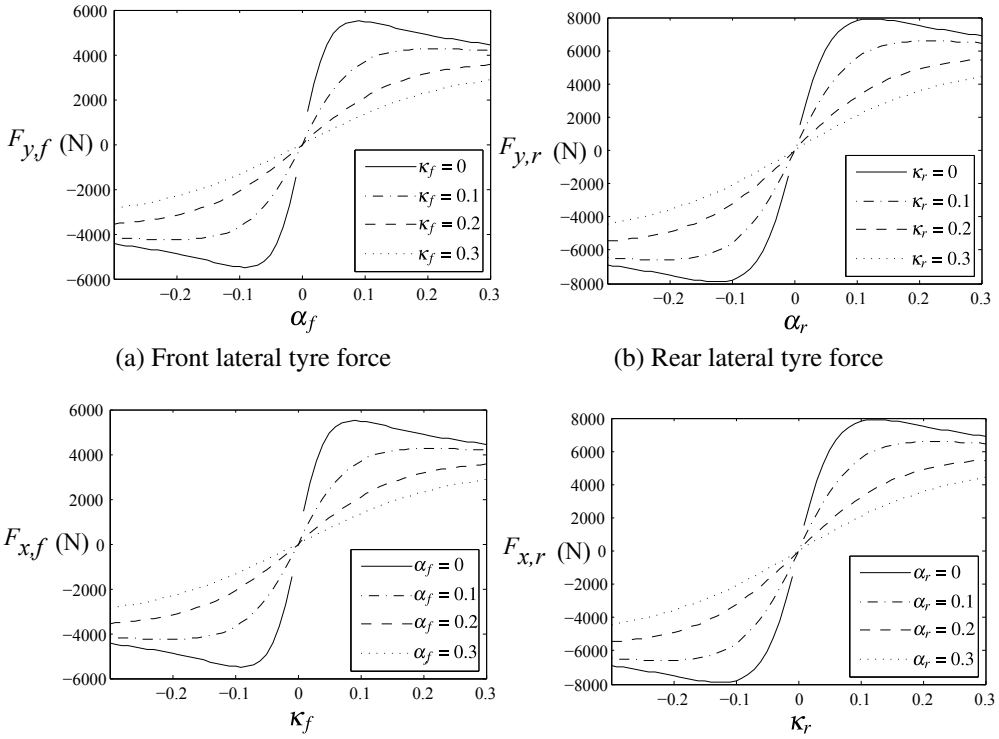
$$P(z) = S_V + D \sin(C \arctan(Bz - E(Bz - \arctan(Bz)))) \qquad (3.4.11)$$

and $z = |\underline{s}| + S_H$. This models the flattening off of the peak tyre force at high slips, when the tyres approach the friction limit. Each of the parameters alter one aspect of the curve. D determines the peak height, the product BCD is the stiffness for low slips, E determines the curvature of the peak and C alters the width of the peak. S_V and S_H are shifts to model the asymmetric effects of ply-steer and conicity [12]. The values of these coefficients, as well as c_1 and c_2, are shown in table 2, and were selected to be identical for the front and rear wheels in this work.

Parameter	Symbol	Value
Stiffness factor	B	1.03
Shape factor	C	1.60
Peak factor	D	1.36
Curvature factor	E	0.00
Horizontal Shift	S_H	0.00
Vertical Shift	S_V	0.00
Cornering Stiffness Parameters	c_1 , c_2	$69\,\mathrm{kN\,rad^{-1}}$, $1.4 \times 10^3\,\mathrm{kN}$

Table 2: Tyre parameters

The resulting tyre force characteristics from these equations are plotted in figure 6 on the facing page. TThe rear tyres generate larger forces because of the rearward biased CoG position.



(a) Front lateral tyre force (b) Rear lateral tyre force

(c) Front longitudinal tyre force (d) Rear longitudinal tyre force

Figure 6: "Magic tyre formula" force characteristics

3.5 Driver Neuromuscular System (NMS)

The driver in reality has a limited bandwidth, and cannot actuate all the frequencies contained in the steering input which he wishes to produce, referred to as the commanded steering input, because of the dynamics of his driver's arms. [13] suggested that the transfer function between the steering wheel torque applied by the driver to the commanded steering wheel angle is second order. Therefore, assuming the steering torque is proportional to and in phase with the true steering wheel angle, the system can be modeled by the second order differential equation:

$$\ddot{\delta}_{sw} + 2\zeta_n \omega_n \dot{\delta}_{sw} + \omega_n^2 \delta_{sw} = \omega_n^2 (\delta_{com} + \delta_{dist}) \tag{3.5.1}$$

where δ_{sw} is the actual steering angle, δ_{com} is the commanded angle, and ζ_n and ω_n are the damping factor and natural frequency respectively [14]. δ_{dist} is the driver's steering disturbance and is described further in section 3.6. The true steering angle is then given by:

$$\delta = \frac{\delta_{sw}}{G_{sw}} \tag{3.5.2}$$

where G_{sw} is the steering mechanism gain. The values for these parameters used in this work are listed below in table 3.

Parameter	Symbol	Value
NMS Natural Frequency	ω_n	$18.85\,\mathrm{rad\,s^{-1}}$
NMS Damping Factor	ζ_n	1.60
Steering Gain	G_{sw}	17

Table 3: Driver NMS parameters

3.6 Disturbances

In equations (3.1.1), (3.1.3) and (3.5.1), the disturbance terms $F_{y,dist}$, $M_{z,dist}$ and δ_{dist} were included respectively. There are numerous potential sources to these disturbances, such as road banking or bumps, differences in traction on the left and right tyres, or aerodynamic loads such as cross-winds. The δ_{dist} term on the other hand comes from the noise in the driver's neurosensory system.

It is the response of the vehicle to these disturbances which will allow the calculation of the state-covariance matrix later in section 5.2, and it will be necessary to specify the statistics of these terms. The steering jitter from the driver could be obtained accurately from a simulator, and the external lateral force and moment disturbances from real track data. However, in this work, for simplicity, it will be assumed that all three are Gaussian, with zero means $\left(\mathrm{E}\left(F_{y,dist}\right) = \mathrm{E}\left(M_{z,dist}\right) = \mathrm{E}\left(\delta_{dist}\right) = 0\right)$, so that when finding the nominal (mean) response of the vehicle with specified steering and drive/brake torque control inputs, this will be with the disturbances terms set to zero. The variance and covariance of these terms must be specified also, but it was assumed that all three are uncorrelated with each other so the covariances were zero. The variances will be set to prespecified values of $\mathrm{var}\left(F_{y,dist}\right) = \sigma^2_{F_{y,dist}}$, $\mathrm{var}\left(M_{z,dist}\right) = \sigma^2_{M_{z,dist}}$ and $\mathrm{var}\left(\delta_{dist}\right) = \sigma^2_{\delta_{dist}}$.

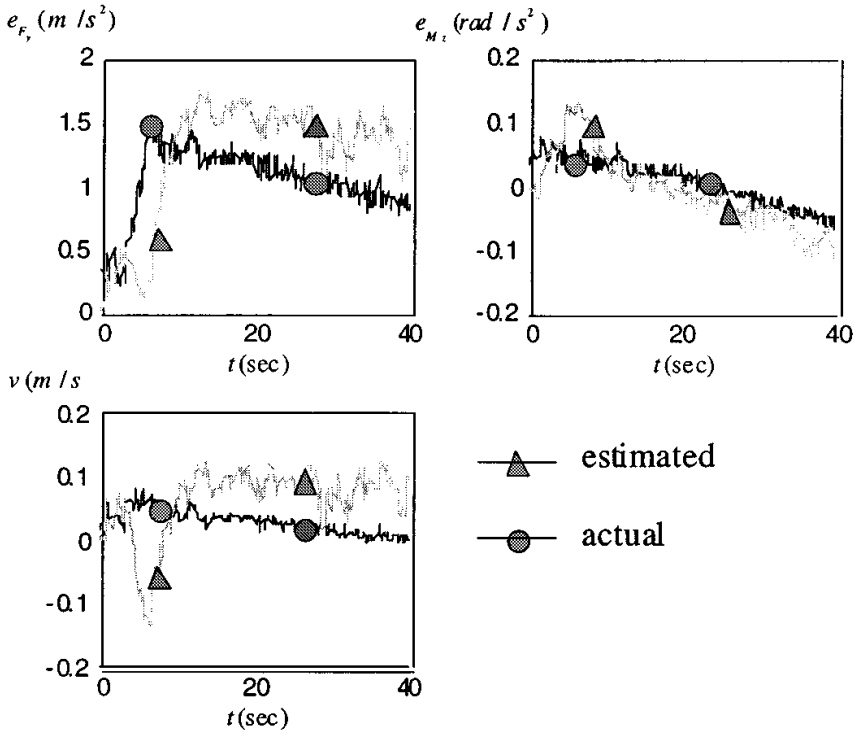


Figure 7: Time histories of lateral velocity and accelerations due to external disturbances with large superelevation and strong winds [15]

The disturbances used in this project were taken from [15]. In this paper, experiments were carried out on an instrumented vehicle on a proving ground, and the lateral and yaw accelerations due to external forces and moments were measured on a 1996 Ford Taurus, which was of a similar mass

and wheelbase to the one used in this model. The road environment was a motorway, so the surface would be similar to that of a race track. Various situations were investigated, but the one deemed to be most representative of a race situation was with a superelevation of 6º and a wind speed of $10\,\mathrm{ms}^{-1}$. The vehicle speed was lower than that used in this project, and the turns were of much larger radii, but this has little affect on order of magnitude of the disturbances. The resulting acceleration profiles are shown in figure 7 on the preceding page.

Since it was assumed that the mean of the disturbances were zero in this work, then the RMS value of these accelerations will equal the standard deviation, achieved using MATLAB's `rms` function. These were then converted into loads, and are listed in table 4. In the case of the steering disturbance, if it is assumed that the vehicle has a peak steering angle δ of 35°, which is typical for such a vehicle, corresponds to a total steering wheel angle travel δ_{sw} of 595° Assuming that the driver has a 1% error, this gives a value for $\sigma_{\delta_{dist}}$ of around 5.95° or 0.1 rad, also listed in table 4.

Parameter	Symbol	Value
Standard Deviation of Lateral Force Disturbance, $F_{dist,y}$	$\sigma_{F_{dist,y}}$	730 N
Standard Deviation of Yaw Moment Disturbance, $M_{dist,z}$	$\sigma_{M_{dist,z}}$	360 Nm
Standard Deviation of Steering Disturbance, δ_{dist}	$\sigma_{\delta_{dist}}$	0.1 rad

Table 4: Statistics of disturbances

3.7 State-Space Model

The tyre slip expressions (3.4.1:3.4.4) can be inserted into those for the tyre forces (3.4.5:3.4.11) . These, which can in turn be put into the equations of motion (3.1.1:3.1.5), along with those for the neuromuscular system (3.5.1:3.5.2) and the lateral path error generating state y in (3.2.2) to give an equation of the form:

$$\dot{x} = f(x,u,w) \tag{3.7.1}$$

where $x = \left[V_y, V_x, \dot{\psi}, \psi, \omega_f, \omega_r, \dot{\delta}_{sw}, \delta_{sw}, y\right]^T$ is the state vector, and $u = [\delta_{com}, T]^T$ is the control input vector, $w = \left[\delta_{dist}, F_{y,dist}, M_{z,dist}\right]^T$ is the disturbance vector. $f(x,u,w)$ is a general non-linear function of x, u and w. One can linearise equation (3.7.1) about the general point (x_0,u_0,w_0) using a first order Taylor series expansion to give:

$$\dot{x} \approx f(x_0,u_0,w_0) + \left.\frac{\partial f}{\partial x}\right|_{x_0,u_0,w_0}(x-x_0) + \left.\frac{\partial f}{\partial u}\right|_{x_0,u_0,w_0}(u-u_0) + \left.\frac{\partial f}{\partial w}\right|_{x_0,u_0,w_0}(w-w_0) \tag{3.7.2}$$

which can then be written in the form:

$$\dot{x} = \mathbf{A}_c x + \mathbf{B}_c u + \mathbf{H}_c w + \mathbf{F}_c \tag{3.7.3}$$

$$\text{where } \mathbf{A}_c = \left.\frac{\partial f}{\partial x}\right|_{x_0,u_0,w_0}, \mathbf{B}_c = \left.\frac{\partial f}{\partial u}\right|_{x_0,u_0,w_0}, \mathbf{H}_c = \left.\frac{\partial f}{\partial w}\right|_{x_0,u_0,w_0}$$

$$\text{and } \mathbf{F}_c = f(x_0,u_0,w_0) - \mathbf{A}_c x_0 - \mathbf{B}_c u_0 - \mathbf{H}_c w_0.$$

This is known as a linear state-space form. $\mathbf{A}_c$, $\mathbf{B}_c$ and $\mathbf{H}_c$ are known as Jacobian matrices with $\mathbf{A}_c \in \mathbb{R}^{n\times n}$, $\mathbf{B}_c \in \mathbb{R}^{n\times m}$ and $\mathbf{H}_c \in \mathbb{R}^{n\times p}$, where n is the number of states, m is the number of inputs p is the number of disturbances respectively (in this case, $n = 9$, $m = 2$ and $p = 3$). $\mathbf{F}_c$ is a vector constant with $\mathbf{F}_c \in \mathbb{R}^n$. To obtain these matrices requires re-linearisation of the model at each time step, to ensure equation (3.7.3) remains accurate. The linearisation point (x_0, u_0, w_0) was always taken as the current nominal state $x_0 = \bar{x}_k$ (with $\psi_0 = 0$, thus fulfilling the requirements specified in section 3.2) and similarly for u_0. In the case of the disturbance vector, w_0 was taken as $w_0 = \bar{w}_k = 0$, since the disturbances have zero mean, as described in section 3.6. However, this term is required, when computing the state-covariance matrix later. This whole process was automated using the functions written by Timings [9]. The non-linear equations could be written in the form in equation as symbolic variables into MATLAB using the Symbolic Toolbox, which could then be analytically differentiated using MATLAB's `jacobian` function. Then all that was required to obtain the Jacobians at each timestep, was to substitute in for x_0, u_0 and w_0.

This is a continuous model, but can easily be converted to give a discrete model of the form:

$$x_{k+1} = \mathbf{A}_k x_k + \mathbf{B}_k u_k + \mathbf{H}_k w_k + \mathbf{F}_k \tag{3.7.4}$$

where $\mathbf{A}_k$, $\mathbf{B}_k$, $\mathbf{H}_k$and $\mathbf{F}_k$ are the discrete time matrices, and k denotes the timestep. Thus, to obtain these matrices at each time step, the model must be relinearised, and then converted into discrete time form, which could be achieved using the `d2cm` function.

4 Driver Model

4.1 Linear Quadratic Control

In order to model the driver response, the general motion of the vehicle in the presence of disturbances is considered. This can equivalently be thought of as a small perturbation term Δx_k about a current nominal state $\bar{x}_k$ (ie. the state when there were no disturbances), with nominal control input $\bar{u}_k$ and disturbance $\bar{w}_k$. Substituting this into equation (3.7.4) gives:

$$x_{k+1} = \bar{x}_{k+1} + \Delta x_{k+1} = \mathbf{A}_k(\bar{x}_k + \Delta x_k) + \mathbf{B}_k(\bar{u}_k + \Delta u_k) + \mathbf{H}_k(\bar{w}_k + \Delta w_k) + \mathbf{F}_k \tag{4.1.1}$$

where Δw_k are the disturbances about the nominal disturbance $\bar{w}_k$ and Δu_k is the control action about the nominal input needed to control these perturbations. $\bar{x}_{k+1}$ is the nominal state vector at time $k+1$. Since $\bar{x}_{k+1} = \mathbf{A}_k\bar{x}_k + \mathbf{B}_k\bar{u}_k + \mathbf{H}_k\bar{w}_k + \mathbf{F}_k$ from (3.7.4), this leaves:

$$\Delta x_{k+1} = \mathbf{A}_k \Delta x_k + \mathbf{B}_k \Delta u_k + \mathbf{H}_k \Delta w_k \tag{4.1.2}$$

Since perturbations about the nominal point $(\bar{x}_k, \bar{u}_k, \bar{w}_k)$ are being considered, the constant term is no longer present. The Δu_k term includes both the steering and drive/brake torque from the the driver to attenuate the disturbances from Δw_k. Since the linearisation point x_0 was taken with $\psi_0 = 0$, then this means that the term Δy in the state perturbation Δx_k does indeed equal the lateral path error e, for the reasons explained in section 3.2.

In order to find the appropriate Δu_k from the driver, and controller was necessary. A linear-quadratic controller (LQR) was selected for this since it can be simply implemented in MATLAB with the `dlqr` function [16], and also tends to produce robust controllers with large gain and phase margins [17]. The aim of this controller is to find an optimal control input Δu_k, so as to minimise a quadratic cost function, which is in general of the form:

$$J = \sum_{k=1}^{\infty} \Delta x_k^T \mathbf{Q} \Delta x_k + \Delta u_k^T \mathbf{R} \Delta u_k \tag{4.1.3}$$

where Δx must be governed by a linear state-space equation of the form in (4.1.2). $\mathbf{Q}$ and $\mathbf{R}$ are the weighting matrices which are constant. This cost function minimises both the deviation from the desired state and the amount of effort from the driver. The solution is a state-feedback controller, with a state feedback gain matrix $\mathbf{K}_k$ so that:

$$\Delta u_k = -\mathbf{K}_k \Delta x_k \tag{4.1.4}$$

The solution is in fact independent of the disturbance terms Δw_k, because if the expected cost is minimised, then, because the variance of Δw_k is constant and the expectation is zero, this only adds a constant to the value function being minimised, and therefore does not alter the optimal Δu_k [18]. Therefore MATLAB's `dlqr` function simply can be used to find $\mathbf{K}_k$, even though it doesn't include the effect of disturbances. This function also assumes, however, that the $\mathbf{A}$ and $\mathbf{B}$ matrices remain constant up until infinity, which will not be the case. However, if it is assumed that the controller is such that the disturbances will be damped out over a short period time, then the main contributions in the cost function will be from small k. For these low values of k, it can be assumed that $\mathbf{A}$ and $\mathbf{B}$ will have changed little from those at the current timestep, as it is close into the future, so it is a good approximation to simply use the $\mathbf{A}$ and $\mathbf{B}$ matrices at the current timestep. It has not yet been discussed how to choose appropriate values for the $\mathbf{Q}$ and $\mathbf{R}$ weighting matrices in the cost function, but this is discussed in the next section.

4.2 Weighting Matrices

In this project, diagonal weighting matrices were used, so that the cost function becomes a sum of squares, thus simplifying the process of tuning the weights. They are therefore of the form:

$$\mathbf{Q} = \text{diag}\,(q_1, q_2, q_3, q_4, q_5, q_6, q_7, q_8, q_9) \text{ and } \mathbf{R} = \text{diag}\,(r_1, r_2)$$

In this work, Bryson's rule was used [19]. This is shown below:

$$q_i = \frac{1}{\text{max. acceptable value of } \Delta x_i^2} \tag{4.2.1}$$

$$r_i = \frac{1}{\text{max. acceptable value of } \Delta u_i^2} \tag{4.2.2}$$

By doing this, this means that if all of the elements of Δx_i and Δu_i are at their maximum values, then all of the terms in the cost function will be equal to one and of equal importance. From this it follows that if an element in Δx or Δu has no limit, then its element in the diagonal of the relevant matrix should be set to near-zero, but the units must be taken into account.

In matrix **Q**, significant weighting was placed on the lateral path error $\Delta y = e$ and attitude error $\Delta\psi$, so as to reduce the deviation from the desired path, due to the disturbances. It was assumed that for these states that suitable maximum values would be of the order of 0.1 m and 0.1 rad respectively. It was also decided that the steering wheel angle should be limited, rather than the $\Delta\delta_{com}$ term in Δu, since it is this physical steering angle that is difficult, rather than the one commanded in the brain. Thus, a limit of 0.1 rad was chosen for $\Delta\delta_{sw}$ and the corresponding weight was placed in **Q**. No restrictions were placed on the other states, so from (4.2.1), this meant small weights were used. They could not be set to zero, as this lead to unobservable modes, so there would be no minimum value for the cost function.

Looking at matrix **R**, the weighting on the extra torque term ΔT was chosen to be high, so as to ensure that the driver would choose to control the disturbances mainly by steering rather than using the accelerator, as the link between the lateral motion and the driver's choice of forward speed is not well understood. It was assumed that it would be acceptable to have ΔT of the order of 10 Nm, which is around 1% of the nominal value. The $\Delta\delta_{com}$ term was made small, since the steering effort was already penalised by the weighting on $\Delta\delta_{sw}$ in **Q**.

This method is good for a first pass, but often needs fine tuning. When these weights were used in the LQR controller for the left-handed turn in figure 8 on the facing page, the resulting attitude error $\Delta\psi$ and lateral path error error $\Delta y = e$ were far smaller than expected, and were deemed unrealistic. Thus the weights for these states were reduced in **Q**. The steering wheel angle had large amounts of high frequency components which the driver could not realistically actuate. Therefore, the element in **Q** for $\Delta\dot{\delta}_{sw}$ was made nonzero, to penalise fast moving steering signals with high frequencies, keeping the term on $\Delta\delta_{sw}$ constant. This overall lead to a reduced steering wheel angle amplitude, and was deemed realisable, as explained in section 4.4. The final parameters are shown in table 5.

Parameter	Symbol	Value
Weighting on $\Delta\psi$	q_3	1
Weighting on $\Delta\dot{\delta}_{sw}$	q_7	2
Weighting on $\Delta\delta_{sw}$	q_8	100
Weighting on $\Delta y = e$	q_9	1
Other diagonal terms	q_1, q_2, q_4, q_5, q_6	10^{-6}

(a) Diagonal Elements of Matrix **Q**

Parameter	Symbol	Value
Weighting on $\Delta\delta_{com}$	r_1	1×10^{-6}
Weighting on ΔT	r_2	0.01

(b) Diagonal Elements of Matrix **R**

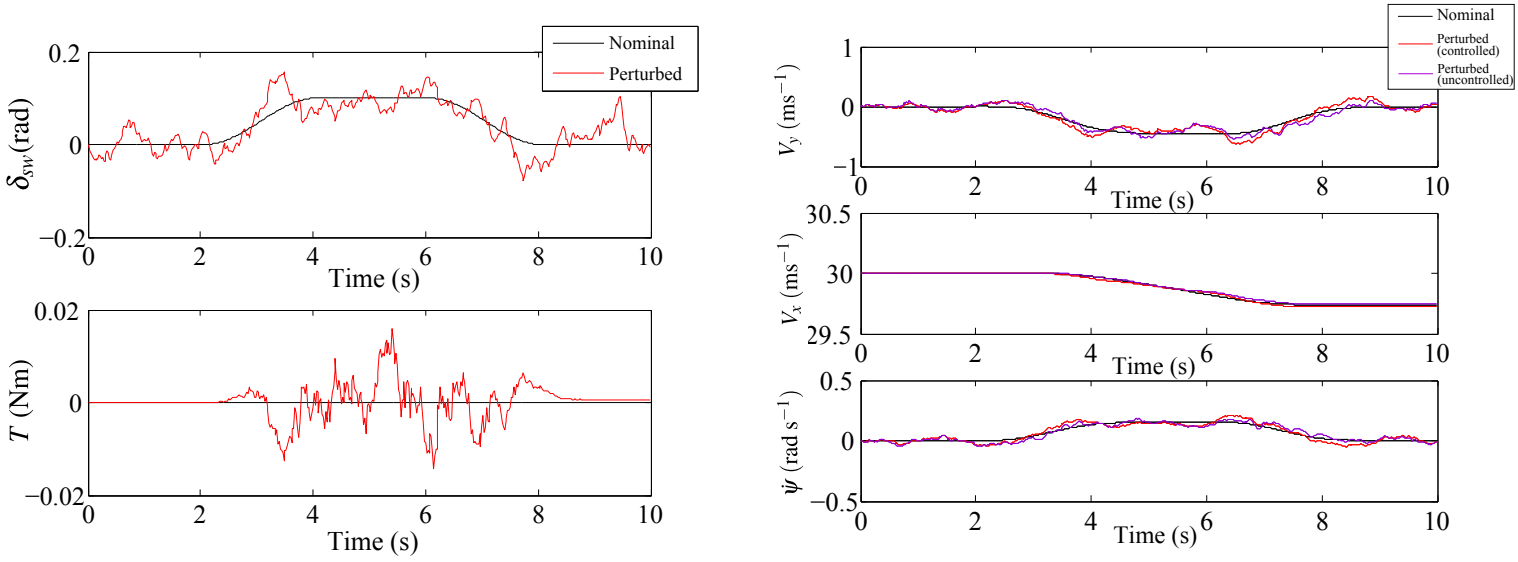
Table 5: LQR weighting matrices elements

4.3 Results

The results for a simulation at $30\,\mathrm{ms}^{-1}$ is shown in figure 8. In figure 8a the nominal controls from the driver are shown in black, and the resulting nominal vehicle states are shown in figure 8b in black.

The vehicle yaws to the left with a negative lateral velocity as expected, indicating that the vehicle model from section 3 is working correctly. The longitudinal velocity reduces slightly during the turn,

since when turning, the lateral tyre force $F_{y,f}$ from the front tyre has a component in the negative x direction, thus decelerating the vehicle slightly. In purple in figure 8b, one ensemble of the perturbed vehicle states due to the disturbances is shown, without any action from the LQR. In red, the perturbed states are shown, but with the perturbed driver controls present (shown in red in figure 8a). These are generally closer to the nominal black states, demonstrating the action of the controller. The longitudinal velocity is peturbed only very slightly form the nominal, and much less than the yaw rate and lateral velocity, as the force and moment disturbances have no component in this direction, and the steering disturbance only causes small longitudinal forces from the front wheel.



(a) Driver control inputs

(b) Resulting Vehicle States

Figure 8: Simulation of a left-handed turn at 30 ms^{-1}

4.4 Bandwidth and Delays

In reality, the driver cannot react instantaneously, due to his cognitive delay [13]. This is separate from the neuromuscular system described in section 3.5. However, if the output from the controller contains mainly lower frequencies below around 1 Hz, then this delay, which will be of the order of 10 ms, is much smaller than the time scale of the signal, which will be of the order of 1 s for frequencies around 1 Hz. It is therefore satisfactory to neglect it. To demonstrate that this is applicable in this case, the power spectral density of the steering wheel angle and torque perturbations $\Delta\delta_{sw}$ and ΔT have been plotted in figure 9 for the same left-handed turn in figure 8. This has been achieved using MATLAB's `periodogram` function. They have been averaged over 1000 iterations so that the general trend can be seen, which would be different from the result from just one iteration, which would be quite noisy. It was found that the -3 dB cut-off frequencies were approximately 0.7 Hz for $\Delta\delta_{sw}$ and 0.5 Hz for ΔT , which are both below the 1 Hz threshold. Thus, it can be argued that it is appropriate to neglect the time delays in the driver model in this work.

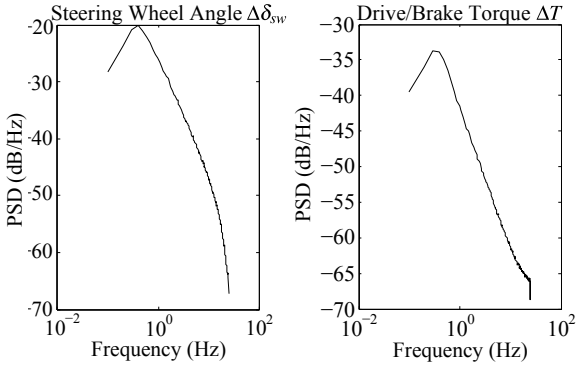


Figure 9: Power spectral density of the driver control inputs for a simulation of a left-handed turn at $30\,\mathrm{ms}^{-1}$

5 Stability Metrics

5.1 Stability Derivatives

One common method already used in the F1 industry for analysing vehicle stability is the use of stability derivatives. These are the instantaneous equivalent stiffness k and damping coefficient λ of a torsional spring and damper system connected to the vehicle, which govern the yaw motion. They are defined in figure 10. M_z is the net yaw moment on the vehicle, $\dot{\psi}$ is the yaw rate of the vehicle, V is the velocity of the vehicle and β is the sideslip angle, and is the angle between the velocity and longitudinal axis of the vehicle. It would be expected from the Routh-Hurwitz stability criterion [7], that it is required that both of these derivatives, k and λ, to be positive for the response not to become unbounded. However, since each vary as a function of time, and there is also closed-loop control, this is not a necessary requirement in this case, and in fact the yaw stiffness is often negative. Despite this, it is expected that if the yaw stiffness becomes less negative or the yaw damping increases, that the vehicle is more stable.

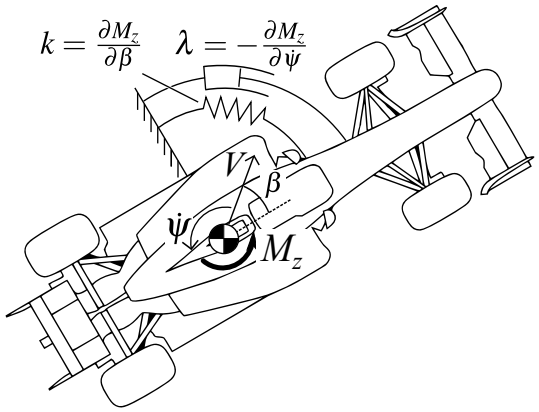


Figure 10: Definition of stability derivatives

For linear tyres, these have the values [4]:

$$\frac{\partial M_z}{\partial \beta} = C_r l_r - C_f l_f \qquad (5.1.1) \qquad\qquad \frac{\partial M_z}{\partial \dot{\psi}} = -\frac{1}{V_x}\left(C_f l_f^2 + C_r l_r^2\right) \qquad (5.1.2)$$

These will be referred to as the yaw stiffness and yaw damping stability derivatives respectively. In order to find these derivatives, it is necessary to numerically differentiate the tyre forces, at the particular vehicle state, with respect to the relevant variable.

5.2 State Variance Matrices

In order to compute the variance of the disturbed system, begin by first taking the covariance of equation (3.7.4) to give

$$\operatorname{cov}(x_{k+1}) = \operatorname{cov}(\mathbf{A}_k x_k + \mathbf{B}_k u_k + \mathbf{H}_k w_k + \mathbf{F}_k) \tag{5.2.1}$$

x_k can again be further split up into a nominal component $\bar{x}_k$ with $\operatorname{cov}(\bar{x}_k) = 0$, and a perturbation Δx_k about this with $\mathrm{E}(\Delta x_k) = 0$. Similarly for u_k and w_k using equation (4.1.1) so as to give

$$\operatorname{cov}(x_{k+1}) = \operatorname{cov}(\bar{x}_k + \Delta x_{k+1}) = \operatorname{cov}(\mathbf{A}_k(\bar{x}_k + \Delta x_k) + \mathbf{B}_k(\bar{u}_k + \Delta u_k) + \mathbf{H}_k(\bar{w}_k + \Delta w_k) + \mathbf{F}_k) \tag{5.2.2}$$

However, the covariance of the nominal components are zero by definition. The variance of the constant is also zero, so (5.2.2) becomes

$$\operatorname{cov}(x_{k+1}) = \operatorname{cov}(\Delta x_{k+1}) = (\mathbf{A}_k \Delta x_k + \mathbf{B}_k \Delta u_k + \mathbf{H}_k \Delta w_k) \tag{5.2.3}$$

Now substituting in for Δu_k using (4.1.4), one obtains

$$\operatorname{cov}(x_{k+1}) = ((\mathbf{A}_k - \mathbf{B}_k \mathbf{K}_k)\Delta x_k + \mathbf{H}_k \Delta w_k) \tag{5.2.4}$$

Since Δw_k contains the disturbances at the kth timestep, this is uncorrelated with the current vehicle state perturbation Δx_k since this has already happened [20], so that equation (5.2.4) can be written as

$$\operatorname{cov}(x_{k+1}) = \operatorname{cov}((\mathbf{A}_k - \mathbf{B}_k \mathbf{K}_k)\Delta x_k) + \operatorname{cov}(\mathbf{H}_k \Delta w_k) \tag{5.2.5}$$

which simplifies to

$$\operatorname{cov}(x_{k+1}) = (\mathbf{A}_k - \mathbf{B}_k \mathbf{K}_k)\operatorname{cov}(\Delta x_k)(\mathbf{A}_k - \mathbf{B}_k \mathbf{K}_k)^T + \mathbf{H}_k \operatorname{cov}(\Delta w_k)\mathbf{H}_k^T \tag{5.2.6}$$

using the covariance identity $\operatorname{cov}(\mathbf{A}b) = \mathbf{A}\operatorname{cov}(b)\mathbf{A}^T$. However, in equation (5.2.3) it was stated that $\operatorname{cov}(x_k) = \operatorname{cov}(\Delta x_k)$ and similarly $\operatorname{cov}(w_k) = \operatorname{cov}(\Delta w_k)$, since the variance of the nominal components are zero. Substituting this into equation (5.2.6), the following equation is finally obtained

$$\operatorname{cov}(x_{k+1}) = (\mathbf{A}_k - \mathbf{B}_k \mathbf{K}_k)\operatorname{cov}(x_k)(\mathbf{A}_k - \mathbf{B}_k \mathbf{K}_k)^T + \mathbf{H}_k \operatorname{cov}(w_k)\mathbf{H}_k^T \tag{5.2.7}$$

It is now clear how the state covariance matrix can be computed at each time step. It propagates with time according to the simple formula in equation (5.2.7); that is, in order to compute the next variance, it is necessary to make use of that at the current timestep. The advantage of this formulation is that the actual response to the disturbance does not need to be computed in order to determine the statistics of the response, so it is very efficient. The only term left unspecified is the covariance matrix $\operatorname{cov}(w_k)$. However, this can be assembled with ease, since in section 3.6, it was stated that the disturbances were assumed to be uncorrelated, and the variances were specified. This means the

matrix $\mathrm{cov}(w_k)$ will be diagonal and of the form:

$$\mathrm{cov}(w_k) = \begin{bmatrix} \sigma^2_{\delta_{dist}} & 0 & 0 \\ 0 & \sigma^2_{F_{y,dist}} & 0 \\ 0 & 0 & \sigma^2_{M_{z,dist}} \end{bmatrix} \tag{5.2.8}$$

Rather than using variances, standard deviations will be used from now onwards, since these are in the same units as the vehicle states, so are easier to interpret. It is possible to confirm that equation (5.2.7) gives the same results as iteratively running the simulation, and taking the standard deviation over the numerous ensembles. The standard deviation computed from 1000 ensembles using MATLAB's `cov` function in shown in turquoise in figure 11, for the same left-handed turn as in figure 8. In blue is the result from using equation (5.2.7). There is a good agreement, since the error is only around 5%, and it is clear that the ensembled line follows the trend of the covariance equation line, thus suggesting equation (5.2.7) is accurate; even for so many ensembles, it has still not fully converged, highlighting another advantage of the using equation (5.2.7).

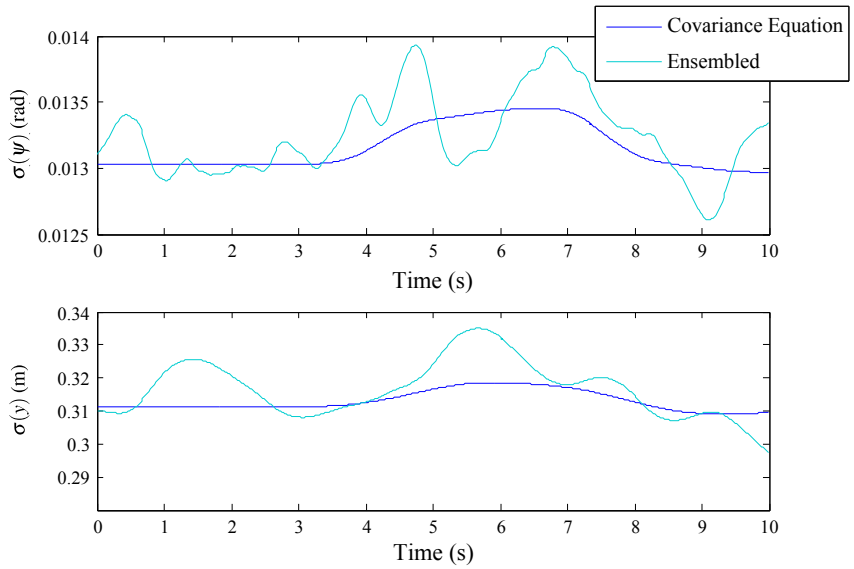
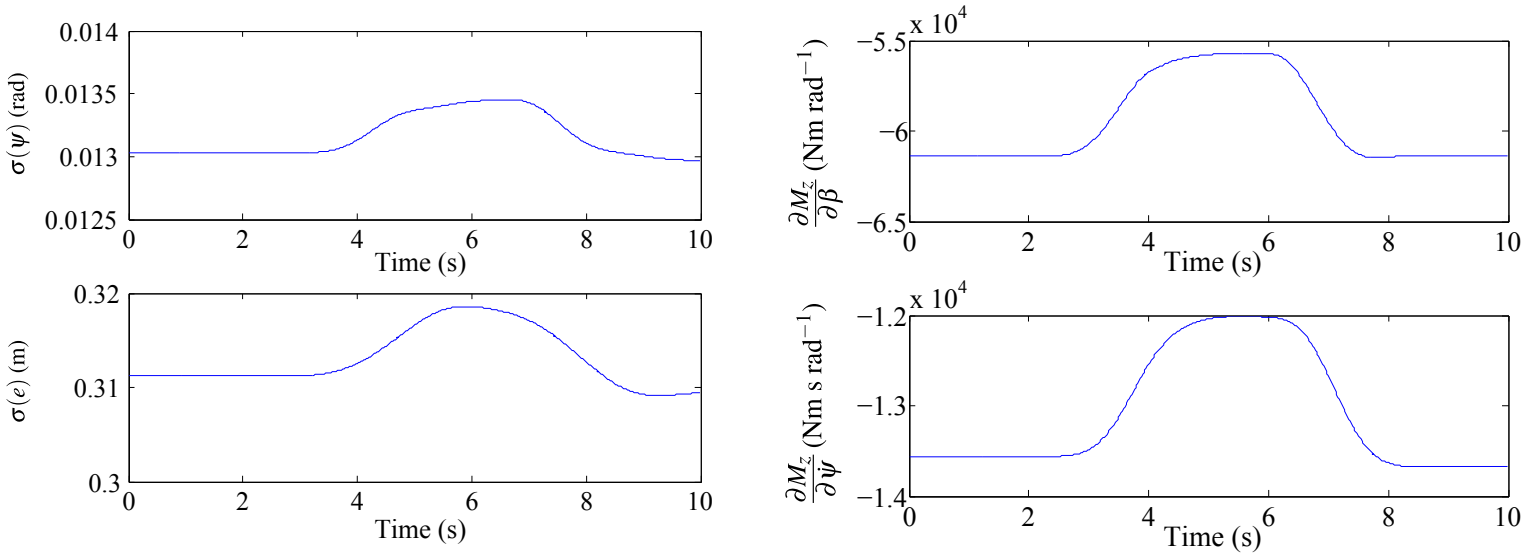


Figure 11: Ensembled state standard deviations of a left-handed turn at $30\,\mathrm{ms}^{-1}$

5.3 Comparison

These metrics are shown in figure 12 for the same left-handed turn in figure 8 on page 21. In figure 12b, the stability derivatives are shown. The stiffness and damping coefficient term goes down during the turn, suggesting that the vehicle will have a more oscillatory response, as might be expected. However, this plot also shows the difficulty in interpreting this information, as the stiffness term is negative for the whole manoeuvre, suggesting it would be unstable, yet it is observed to be practically stable. Also, during the turn, the yaw damping reduces, suggesting the vehicle is less stable, whilst the yaw stiffness becomes less negative, which is a stabilising effect, so there is a contradiction, adding to the ambiguity. By comparison, the state standard deviations in figure 12a are much

easier to interpret. The standard deviation of the lateral path error and yaw angle have been plotted, since these have easy physical interpretations; particularly the lateral path error, since this allows us to quote the maximum deviation from the nominal path due to these disturbances to a certain level of confidence. For this reason, only this standard deviation will be used in the remainder of the work. During the turn, these standard deviations rise, suggesting the disturbances propagate more readily, as expected, so the vehicle appears stable. The action of the controller can also be seen, since the standard deviations settle back to zero after the manoeuvre, so objective 1 has been achieved, and the problems from [1] have been resolved. Since there is an overall destabilising effect during the turn, this implies that the yaw damping reduction is perhaps more significant than the less negative yaw stiffness.



(a) State Standard Deviations

(b) Stability Derivatives

Figure 12: Stability metrics for a left-handed turn at $30\,\mathrm{ms}^{-1}$

6 Controllability Metrics

6.1 Controllability Derivatives

In the same way in which certain derivatives can help quantify the stability, there are equivalent derivatives, known as controllability derivatives, which can be used to describe how easy the car is to drive. The two which were selected for further investigation from [4] were $\frac{\partial F_y}{\partial \delta_{sw}}$ and $\frac{\partial M_z}{\partial \delta_{sw}}$ were F_y and M_z are the net lateral forces and moments on the vehicle, and δ_{sw} is the true wheel steering angle. These can be considered as stiffnesses in the same way as the stability derivative $\frac{\partial M_z}{\partial \beta}$, as they give a measure of the controlling lateral force and moment for an increment in steering angle, thereby characterising the controllability. In the case of linear tyres, these have the follow values [4]:

$$\frac{\partial F_y}{\partial \delta_{sw}} = C_f \qquad (6.1.1) \qquad\qquad \frac{\partial M_z}{\partial \delta_{sw}} = l_f C_f \qquad (6.1.2)$$

where C_f and C_r are the stiffnesses of the front and rear tyres in the linear region. These controllability derivatives will be referred to as the force and moment "stiffness" terms respectively. They require numerical differentiation of the front tyre force with respect to the steering wheel angle.

6.2 Control Variance Matrix

In order to assess the controllability of the vehicle, it was decided to attempt to extend the covariance method to the control inputs, thus giving a measure of the driver's effort. The initial quantities of particular interest were the steering wheel rate and the drive/brake torque. The steering wheel rate was chosen over the actual steering wheel angle, since the physical difficulty arises from quickly changing steering wheel angles, rather that simply the amplitude [21]. This quantity can already be calculated from equation (5.2.7) since $\dot{\delta}_{sw}$ is one of the vehicle states. However, this is not the case for the drive/brake torque. This requires computation of the variance of the vector u_k.

In order to achieve this, u_k is split into a nominal and peturbed component in the same way as in equation (5.2.2) so that:

$$\mathrm{cov}\,(u_k) = \mathrm{cov}\,(\bar{u}_k + \Delta u_k) = \mathrm{cov}\,(\Delta u_k) = \mathrm{cov}\,(-\mathbf{K}_k \Delta x_k) \qquad (6.2.1)$$

using equation (4.1.4), and again noting the covariance of the nominal part is zero by definition. Using the covariance identity that $\mathrm{cov}\,(\mathbf{A}b) = \mathbf{A}\mathrm{cov}\,(b)\,\mathbf{A}^T$ and that $\mathrm{cov}\,(x_k) = \mathrm{cov}\,(\Delta x_k)$ as before in (5.2.3), (6.2.1) becomes:

$$\mathrm{cov}\,(u_k) = \mathbf{K}_k \mathrm{cov}\,(x_k)\,\mathbf{K}_k^T \qquad (6.2.2)$$

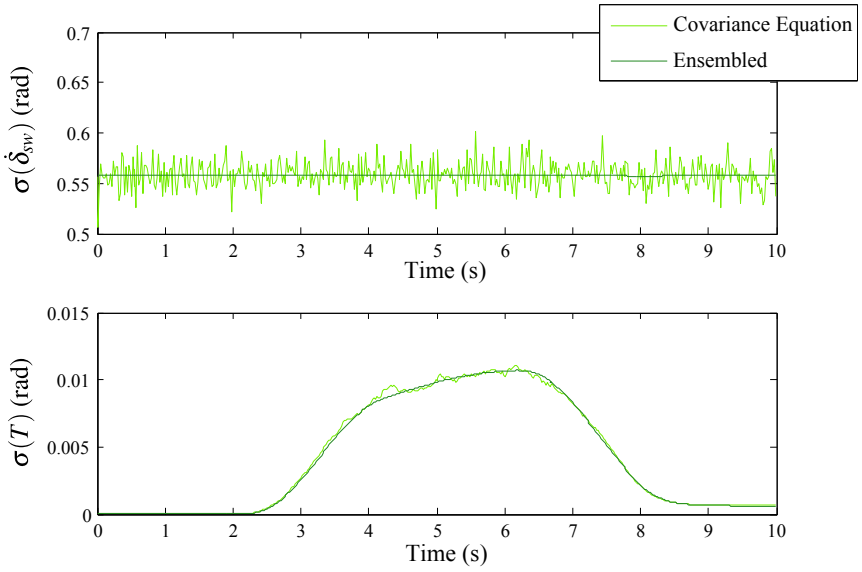


Figure 13: Ensembled control input standard deviations of a left-handed turn at $30\,\mathrm{ms}^{-1}$

Thus, once the state-covariance is computed at each timestep, the covariance matrix of the input vector can be found by simply using equation (6.2.2). As before in section 5.2, the results over 1000 iterations for the same left-handed turn as in figure 8, again using MATLAB's `cov` function, are shown in figure 13 on the preceding page in light green. In dark green, the result from using equation (6.2.2) is shown. It is clear that there is again a good agreement, thus suggesting (6.2.2) is accurate.

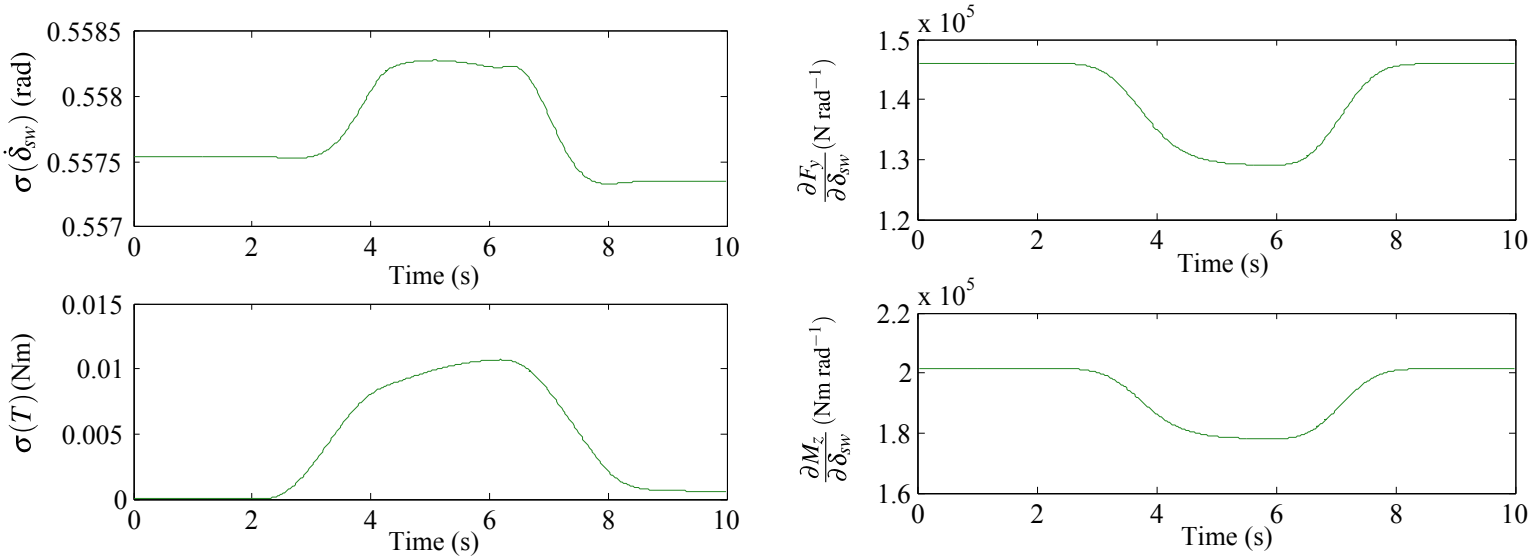
6.3 Comparison

These metrics are shown in figure 14 for the same left-handed turn in figure 8. In figure 14b, the controllability derivatives are shown. Both of the stiffness terms $\frac{\partial F_y}{\partial \delta_{sw}}$ and $\frac{\partial M_z}{\partial \delta_{sw}}$ reduce during the turn, suggesting that driver will have to turn the steering wheel with a greater amplitude to control the vehicle. For these plots, there are no ambiguous negative portions, since by definition, this is not possible. The top graph of figure 14a showing the standard deviation of the steering wheel velocity $\dot{\delta}_{sw}$, agrees well with this behaviour. It settles to a higher level during the turn and then returns to zero, suggesting the driver would have to turn the steering wheel faster during the turn, as one might expect.

The standard deviation of the drive/brake torque is shown in the bottom graph of figure 14b, which starts zero, since there are only lateral disturbances on the vehicle, so braking/accelerating is not required to damp them out. During the turn however, the drive/brake torque settles to an approximately constant positive value. This was found to be because during the turn, the steering disturbance leads to a variation in the front wheel lateral force $F_{y,f}$, which has a component in the longitudinal direction when the nominal steering wheel angle is non-zero. Therefore, disturbances in the longitudinal velocity build up, which can only be damped out by accelerating or braking. However, this torque term torque ΔT term is in no way meaningful in reality, since no model for the driver's speed control was included in the LQR model. The only reason that the output is not zero is because the weighting in matrix $\mathbf{R}$ in the cost function was made very high, but still finite. For this reason, this standard deviation was ignored in the remainder of the project.

It can be argued that as with the stability, the standard deviations of the controls are easier to interpret than the derivatives, because they are expressed in the units of the controls themselves. They can give also a better impression of the driver steering effort, since the standard derivation of the steering velocity was used, but the controllability derivatives do not penalise fast moving controls in the same way. When one considers the computational effort, the standard deviation method appears superior, since the derivatives required extra numerical differentiation of the forces and moments, whereas the standard deviations require only the equations (5.2.7) and (6.2.2), and makes use of the state variance matrix already computed. However, both methods do not depict the longitudinal controllability in a meaningful way, but each could be altered so that this was the case; for example, if a model of driver speed control was used, the standard deviation of the drive/brake torque could be used, and derivatives such as $\frac{\partial F_x}{\partial T}$ could have been used. In any case, it can be argued that objec-

tive 2, which was to extend the stability metrics to allow the controllability to be assessed, has been successfully completed.



(a) Control Input Standard Deviations

(b) Controllability Derivatives

Figure 14: Controllability metrics for a left-handed turn at 30 ms^{-1}

7 Parameter Study

7.1 Methodology

Now that suitable metrics for characterising the stability and controllability of the vehicle have been developed and investigated, it was deemed useful to apply them in a parameter study, so as to isolate the effect of each parameter on the handling and performance of the vehicle. This was achieved by using a standard track geometry, and then altering the parameters of the vehicle. For each setup, the optimal trajectory must be found, and then the controllability and stability were then computed. This whole process is best demonstrated by a flow chart as shown in figure 15 on the facing page. Only one parameter was altered at one time, around the nominal parameters shown in section 3, so the causes of any trends found can be isolated.

7.2 Track Geometry

The same left-handed 90° bend was used for the whole of the parameter study, of the dimensions shown in figure 16. There is a short straight section of 360 m, followed by a 90° bend of length 100 m, and of a constant radius of 63.7 m. A very long straight section follows, with the simulation terminating 40 m into this. The vehicle starts on the left hand side of the track on the initial straight section, at a speed of 30 m s^{-1}, and the width of the track is 10 m, which remains constant throughout. The width of the vehicle however, is neglected, so the vehicle trajectory may touch the edges of the track. The sectors of the manoeuvre are also highlighted.

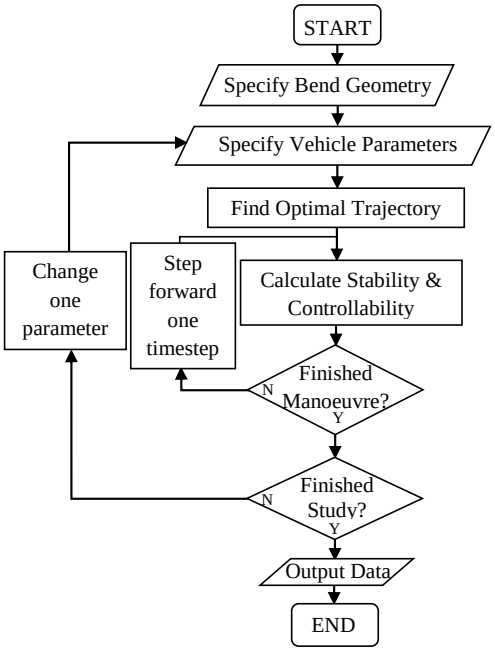


Figure 15: Flow chart of parameter study

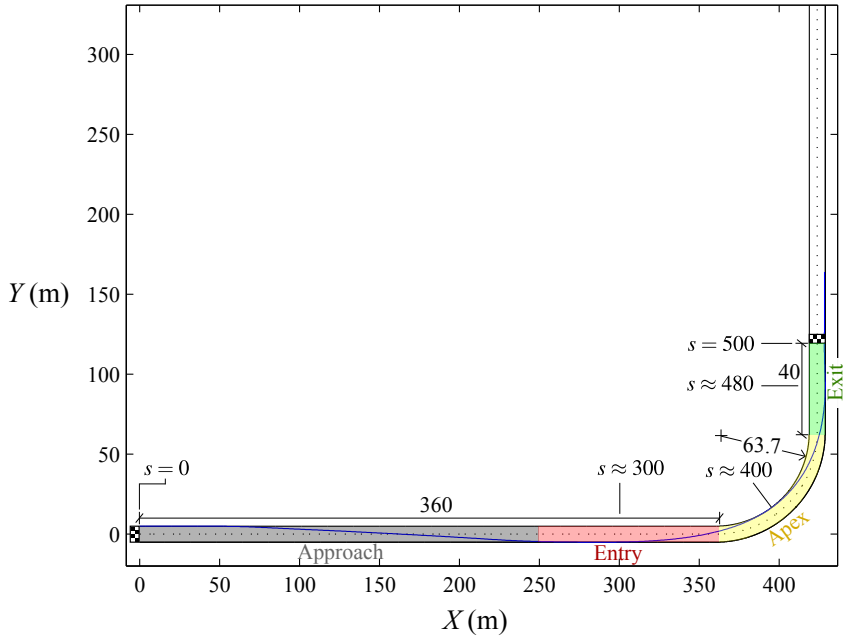


Figure 16: Track geometry used for the parameter study

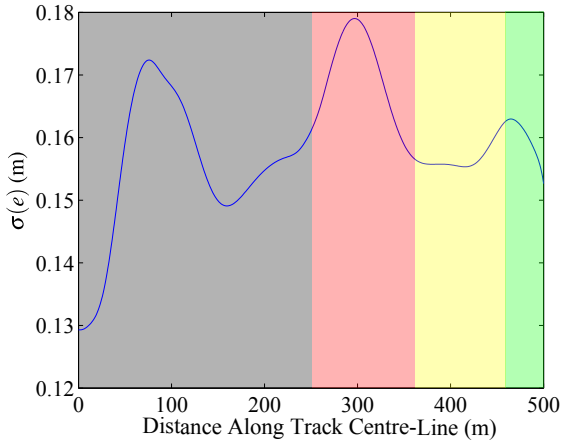
7.3 Computation of Optimal Vehicle Trajectories

In order to achieve objective 3, which was to be able to find the optimal vehicle trajectory around specific track geometries, Timings' Lapsim tool [9] was used. This generates the required steering and drive/brake torque controls required to navigate the vehicle around a given track geometry and vehicle set-up, subject to constraints in the minimum time. This is achieved by formulating the problem as a quadratic program, for which there are standard solvers. These control inputs can then be fed into the original vehicle time-domain simulation to generate the stability and controllability metrics.

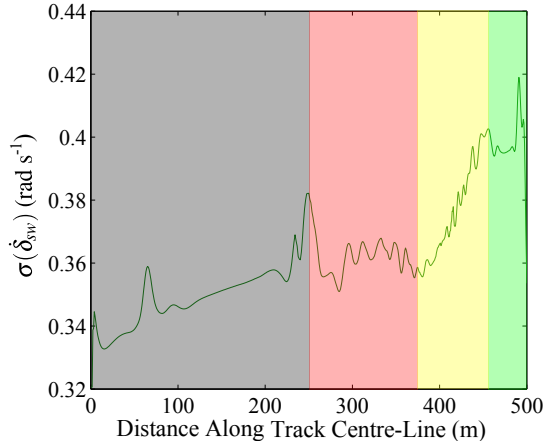
The resulting optimal trajectory for the nominal vehicle setup is also shown in figure 16. As expected, the vehicle moves over to the outside of the track, and then clips the apex, so as to take the widest arc through the turn. After exiting the turn, the vehicle remains on the right hand edge of the track, and continues to travel in a straight line, because there is no turn ahead.

7.4 Results for the Nominal Vehicle Parameters

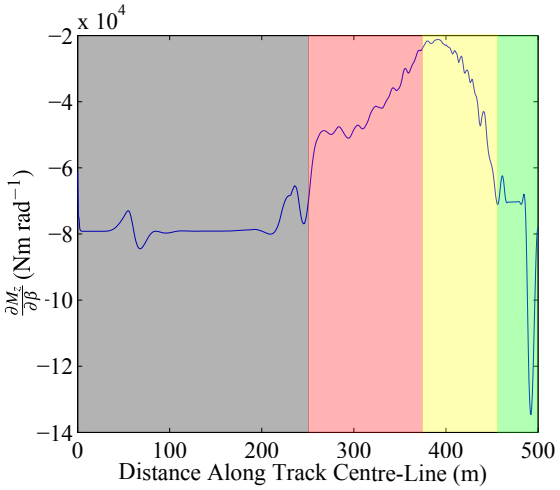
The Lapsim tool was first run with only the nominal vehicle parameters listed in tables 1, 2 and 3, in order to establish and explain the prominent features in the various stability and controllability metrics, and to also provide a comparison in the full parameter study in section 7.5. This also allowed objective 4 to be fulfilled. These results are shown in figure 17 on the next page. The key features will now be discussed.



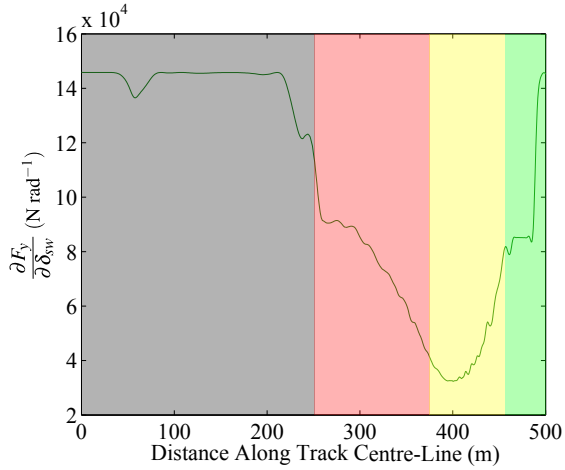
(a) Standard deviation of lateral path error



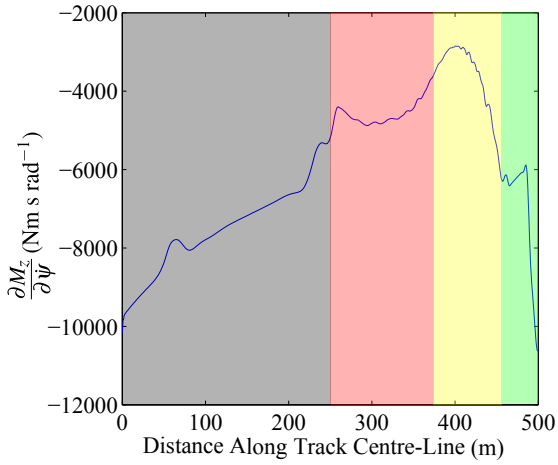
(b) Standard deviation of steering wheel velocity



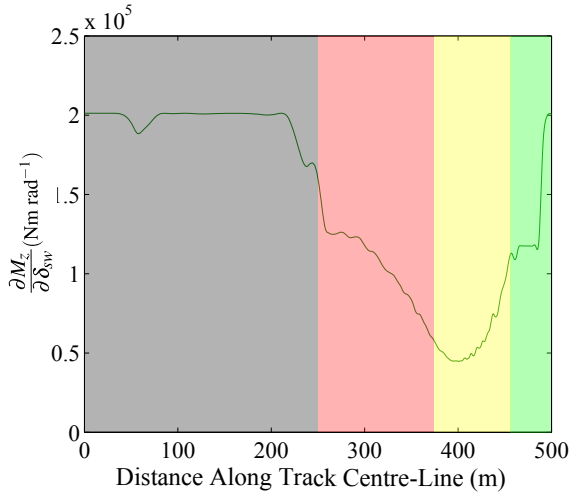
(c) Yaw stiffness stability derivative



(d) Force steering "stiffness" controllability derivative



(e) Yaw damping stability derivative



(f) Moment steering "stiffness" controllability derivative

Figure 17: Stability and controllability metrics for the nominal vehicle setup on an optimal trajectory around a 90° bend

Stability

Approach ($s \lesssim 250\,\mathrm{m}$) Looking at the standard deviation of the lateral path error first in figure 17a, there is an initial large peak at around $s \approx 75\,\mathrm{m}$ because there is a large peak in the steering input here, to begin moving the vehicle to the outside of the track. This has the tendency to reduce the effective front tyre stiffness, which allows disturbances to propagate more. This can also be seen in the yaw stiffness in figure 17c which becomes less negative, and the drop in damping in figure 17e, because both depend on the effective tyre stiffness from (5.1.1) and (5.1.2). Next, on approach to the turn, the lateral error starts at a lower value, and gradually begins to rise. At the same time, the yaw damping in figure 17e begins to reduce gradually, so tallies with this behaviour well. This is because this is where the vehicle begins to brake, so both the front and rear tyres begin to saturate. However, both tyres are affected roughly equally, since the brake balance was coincidentally chosen in proportion to each of the vertical tyre loads. From (5.1.2), these changes are additive for the yaw damping reduces, but because of the minus sign in (5.1.1), these effects seem cancel out for the yaw stiffness, as shown in figure 17c.

Entry ($s \approx 300\,\mathrm{m}$) At this point is the largest peak in the lateral error. There is also a step reduction in the yaw damping in figure 17e, and the yaw stiffness becomes slightly less negative figure 17c. The reasons for this are that here, the braking torque is high and there is a peak in the steering input, leading to some tyre saturation.

Apex ($s \approx 400\,\mathrm{m}$) At this point, the lateral error settles at the value just before entry into the turn, and remains constant, suggesting that the vehicle is relatively stable. This can be explained by how the yaw stiffness in figure 17c becomes less negative here, but on the other hand, the yaw damping becomes very low here too in figure 17e. This is because the lateral acceleration, and hence tyre slips are at their highest here, so the tyres are very close to their limit. This also shows the ambiguity in these derivatives however, since despite the two competing effects, there appears to be an overall stabilising effect. This discrepancy can be explained by the reduction in the controllability derivatives in figures 17d and f, so the steering disturbances propagate less.

Exit ($s \approx 480\,\mathrm{m}$) On exit, there is another peak in the lateral error in figure 17a, larger than that on entry. At this point, the driver has already begun accelerating, so the rear tyre stiffness reduces giving the vehicle an oversteer characteristic. The driver therefore has to use opposite lock, to navigate out of the turn. This leads to a reduction in the front tyre stiffness, affecting both derivatives. However, because of the dependence on the velocity in (5.1.2), which is lower than on entry, the effects cancel out in the yaw damping. After the turn, the control inputs are the same as they were at the beginning of the approach, which is reflected in the metrics.

Controllability

Approach ($s \lesssim 250\,\mathrm{m}$) On approach to the turn, the standard deviation in the steering wheel velocity in figure 17b increases gradually, with a peak where there were none in the lateral error. This shows the driver's effort to control the disturbances here. This is reflected in the controllability derivatives in figures 17d and (f), because at this point, there was a peak in the nominal steering input, leading to a high front slip angle, reducing the front tyre stiffness slightly, reducing the derivatives from (6.1.1) and (6.1.2). The steering wheel velocity continues to grow as the vehicle is unstable but the controllability derivatives remain flat; they only reflect the magnitude of the effect of the steering wheel angle, and not how much the driver may need to turn it to control disturbances, highlighting their limitation. At the end of the approach, there is a very sharp rise in the steering wheel velocity where controllability derivatives have dropped. This is because the braking torque is high and there is a peak in the nominal steering input, reducing the effective front tyre stiffness considerably.

Entry ($s \approx 300\,\mathrm{m}$) At entry, the steering wheel velocity settles at a high value, slightly lower than at the end of the approach, suggesting the controllability has reduced. However, the controllability derivatives in figures 17d and f also reduce, as the braking torque increases further, suggesting the vehicle is more controllable. This disagreement could be because the lateral error is high here, so the cost function limits how much more driver effort can be put in, again highlighting a limitation of the controllability derivatives.

Apex ($s \approx 400\,\mathrm{m}$) At the apex, and just after it, the steering wheel velocity in figure 17b begins to rise. This agrees with the controllability derivatives in 17d and f which are both at their lowest here; the tyres are near saturation, which means to attenuate the forces and moment disturbances, the driver must work much harder. However, this also has the advantage that the steering disturbances do not propagate so readily, stabilising the vehicle.

Exit ($s \approx 480\,\mathrm{m}$) On exit, the steering wheel velocity in figure 17b is at its highest, and higher than at the apex, caused by the high instability in the vehicle, whereas the controllability derivatives are slightly higher than at the apex, because the vehicle begins to accelerate and there was also a peak in the nominal steering input, so there is some tyre saturation.

7.5 Results with Varying Vehicle Parameters

In order to continue the assessment of the metrics, further simulations were run along optimal trajectories, which was objective 4. However, the vehicle parameters were now varied, isolating the effects of each parameter, which was objective 5. Throughout, the nominal vehicle set-up is highlighted as a thick line on the stability and controllability plots, and as a circle on the manoeuvre time plots. Each section will begin with an overall summary, and then continue with some more specific observations and explanations.

7.5.1 Brake Balance

The optimum from this section was selected as the nominal value throughout the project. The results for the range of brake balances are shown in figures 18, 19 and 20. In general, it was concluded that rear biased vehicles are less stable and controllable on entry, but front biased vehicles are less stable and controllable on exit. Therefore, the brake balance which optimises the performance, around 0.4 in this case, also seems to lead to the best handling performance.

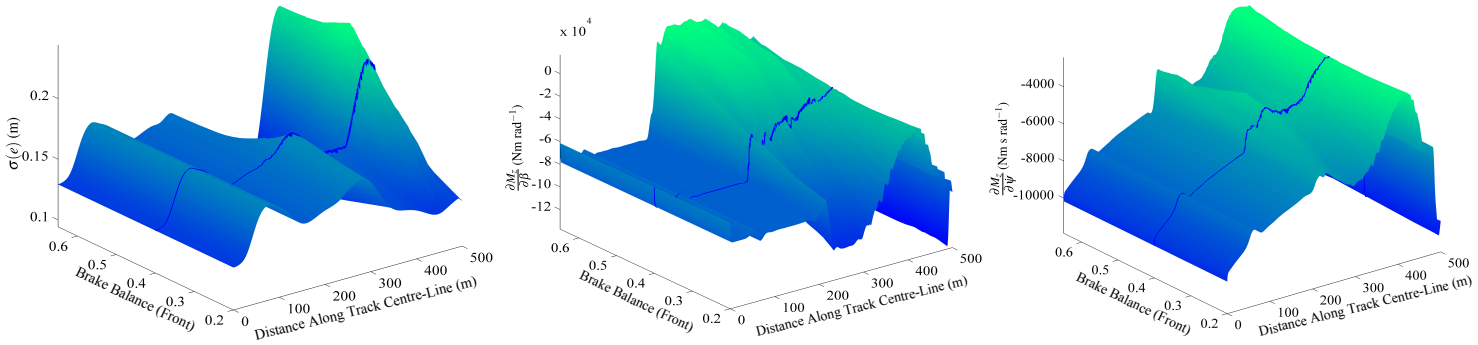
Stability

Approach ($s \lesssim 250\,\mathrm{m}$) It is clear from the lateral path error standard deviation in figure 18a and the stability derivatives in figures 18b and c, that for up until entry, the stability is independent of the brake balance. This is because the vehicle does not brake here, so the brake balance is irrelevant.

Entry ($s \approx 300\,\mathrm{m}$) On entry, the forward brake biased vehicles are more stable, with both a less negative yaw spring stiffness, and a smaller lateral path error standard deviation. This was found to be because the front tyres, which already have larger lateral slips, become nearer to saturation, reducing the lateral stiffness, and the reverse for the rear tyres. For the yaw stiffness term in figure 18b these changes are additive, due to the minus sign in (5.1.1), stabilising the vehicle. However, the damping in figure 18c varies little, because the plus sign in (5.1.2) means the changes to the front and rear tyre stiffnesses approximately cancel.

Apex ($s \approx 400\,\mathrm{m}$) At the apex, there is little variation, since the tyres are fully saturated for all vehicles in the lateral direction.

Exit ($s \approx 480\,\mathrm{m}$) There is a very significant difference in behaviour here. The front biased vehicles have a much higher lateral path error, than for the rear biased vehicles. This effect is not visible in the stability derivatives, but was found to be because the racing line is tighter, and the braking is more harsh for these setups.



(a) Standard deviation of lateral path error (b) Yaw stiffness (c) Yaw damping

Figure 18: Variation of stability with brake balance

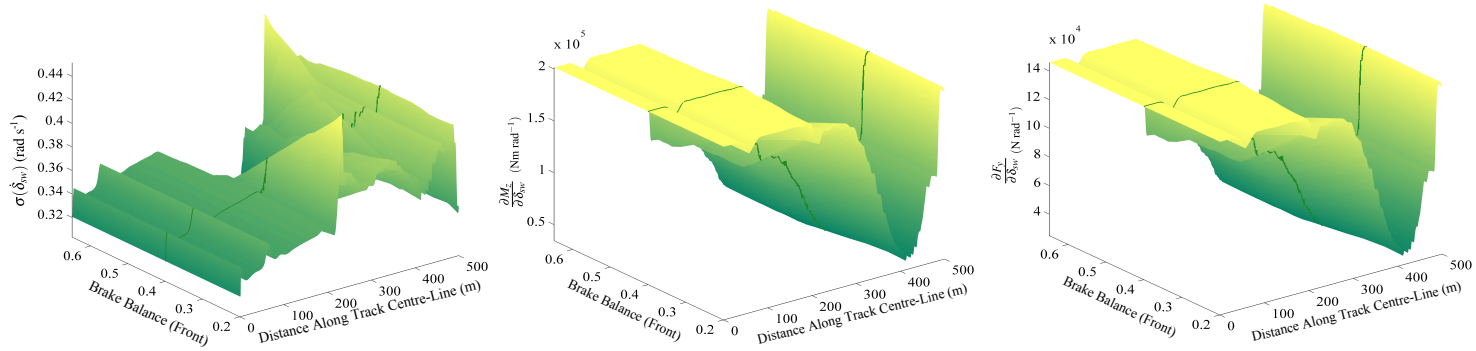
Controllability

Approach ($s \lesssim 250\,\mathrm{m}$) There is again little variation for the approach phase of the manoeuvre.

Entry ($s \approx 300\,\mathrm{m}$) There is a peak in the steering wheel velocity in figure 19a here, for rear biased vehicles. This can be explained from the controllability derivative stiffness terms in figure 19b and c, are both higher on entry for the rear biased vehicles, there are smaller longitudinal slips on the front tyres. This means the steering disturbances propagate more readily, so the driver must do more to control them.

Apex ($s \approx 400\,\mathrm{m}$) At the apex, there is again little variation, since the tyres are fully saturated.

Exit ($s \approx 480\,\mathrm{m}$) There is a peak for front bias vehicles here. This was found to be because the front biased vehicles took a straighter line due the reduced braking performance, so turned more sharply on exit. This feature was too transient to show in the controllability derivatives.



(a) Standard deviation of steering wheel velocity

(b) Moment steering "stiffness"

(c) Force steering "stiffness"

Figure 19: Variation of controllability with brake balance

Performance At a value of $b_f \approx 0.4$, the longitudinal forces are spread in proportion to the vertical tyre loads, so the front and rear tyres are further from saturation. This means the vehicle can brake later and take a tighter racing line, thus leading to a reduction in the manoeuvre time, shown in figure 20. Around this value, the braking performance is compromised due to saturation and hence the manoeuvre time is worse.

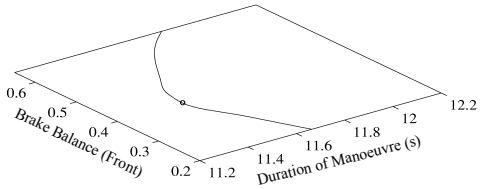


Figure 20: Variation of performance with brake balance

7.5.2 Centre of Gravity Position

The centre of gravity position was varied about the nominal setup, whilst keeping the wheelbase and all other parameters constant. This would otherwise alter the braking performance, as the static loads F_z on each axle vary, in turn altering the size of the friction circle for each tyre. To counteract this, the brake balance had to be varied in proportion with the change in vertical loading F_z, since the size of the friction circle F_p is approximately proportional to F_z for low F_z. Since F_z consists only of the static weight terms, the braking force from each axle is proportional to the product of the appropriate brake balance portion (ie b_f for the front or $\left(1-b_f\right)$ for the rear) and axle to CoG distance (ie l_r for the front and l_f for the rear). One eventually obtains:

$$b_f = \frac{L-2l_{f,0}}{L-2l_f}\, b_{f,0} + \frac{l_{f,0}-l_f}{L-2l_f} \tag{7.5.1}$$

where $l_{f,0}$ is the original distance between the front axle to the CoG, and $b_{f,0}$ is the original brake balance.

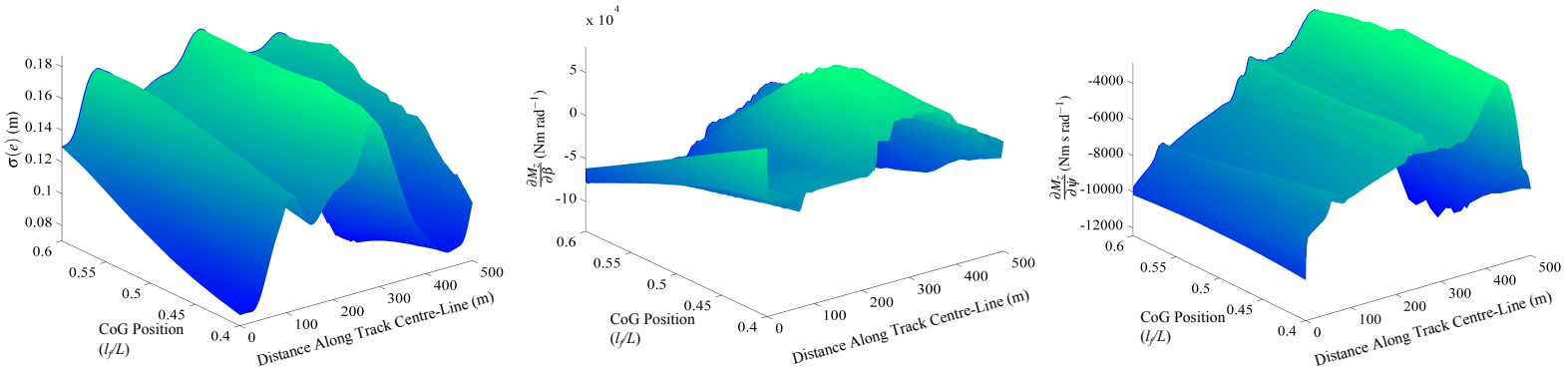
It was not possible to make $l_f > 0.6L$, and this gave the vehicle such a strong understeer characteristic, so that there was no convergent optimal trajectory. Also, making $l_f < 0.4L$, made the simulation unstable also, since this gave the vehicle a strong oversteer characteristic. It was concluded that the forward biased vehicles were slightly more stable, but the rearward biased vehicle were more controllable, with little change in the performance, although for centrally placed CoG's, the performance was severely reduced. However, given the improved controllability makes the vehicle more manoeuvrable, the rearward biased vehicle may be chosen as the optimum, avoiding the instabilities associated with oversteering vehicles.

Stability

Approach ($s \lesssim 250\,\mathrm{m}$) From the standard deviation of the lateral path error shown in figure 21a, the more frontwards the CoG is placed, the more stable the vehicle is. This is also reflected in the yaw stiffness in figure 21b which is less negative, and the lateral error reduces. This is because reducing l_f reduces the moment arm of the front tyre, and vice versa for the rear tyre, reducing the stiffness from (5.1.1). The effects appear to cancel for the yaw damping in figure 21c.

Entry ($s \approx 300\,\mathrm{m}$) **& Apex** ($s \approx 400\,\mathrm{m}$) Similar trends are observed at entry and at the apex, but the increase in stability for front-biased vehicles is less marked. This is because as l_f is reduced, this increases l_r, so thus increasing the rear lateral slip, eventually saturating it. The stiffness of the front tyres did not vary significantly with l_f, since the slip remains high, no matter which l_f is used, due to the steering angle. Therefore the yaw stiffness for front biased vehicles peaks off, meaning the stability doesn't improve so much here.

Exit ($s \approx 480\,\mathrm{m}$) Similar trends to the approach are now observed. This is because the torque is now as it was on approach. This means the rear tyres do not saturate, so the yaw stiffness does not peak off for front biased vehicles like at the apex.



(a) Standard deviation of lateral path error (b) Yaw stiffness (c) Yaw damping

Figure 21: Variation of stability with centre of gravity position

Controllability

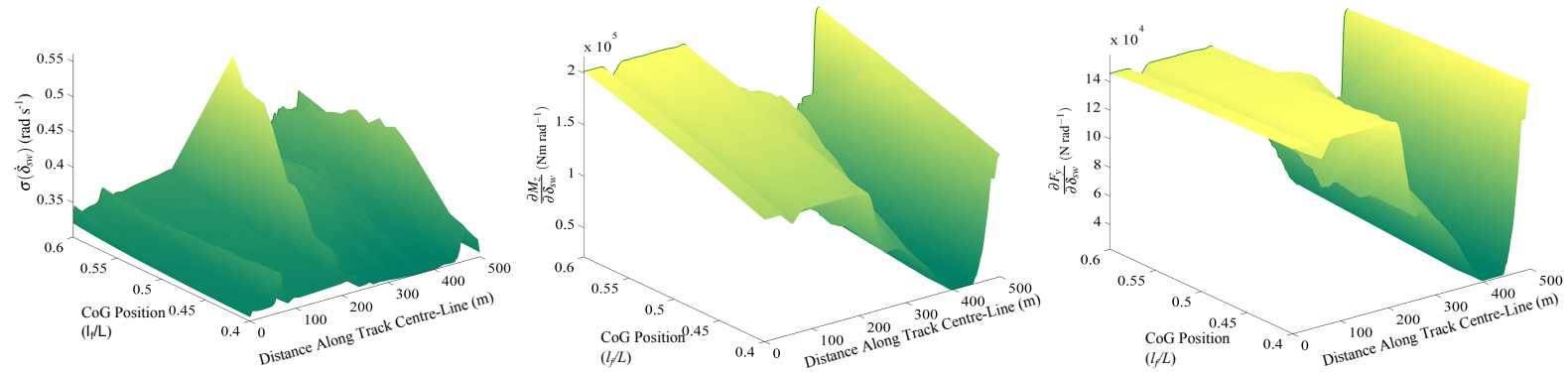
Approach ($s \lesssim 250\,\mathrm{m}$) There is very sharp peak in the standard deviation of the steering wheel velocity in figure 22a centered around the point where the CoG is in the middle of the vehicle, not observed in the stability metrics. When the CoG is in the middle, no value of brake balance will give the desired braking performance, which can be seen from (7.5.1); if l_f is a finite distance below $L/2$, and above $L/2$, $b_f \to 0$. Therefore, in each case, only one axle is used to brake, so the braking performance is reduced, and whereas the acceleration is not so severely affected. This meant that the racing line for these vehicles was to brake sooner, and take a straighter line through the turn and at higher speed. This means there was a peak in the yaw rate just before entry, sooner that for other vehicles, when the yaw stiffness was more negative, and hence less stable. The attitude errors (not shown) grew more readily here, ultimately leading to the driver to work harder to correct this error.

This effect is not shown in the controllability derivatives. The force stiffness in figure 22c does not change, whereas there is a linear change in the moment stiffness in figure 22b, as the moment arm of the front tyre changes linearly. This highlights this same limitation of the controllability derivatives, that they do not account for the inherent vehicle instability.

Entry ($s \approx 300\,\mathrm{m}$) There is only a small variation in the steering wheel velocity here with CoG position, as the racing lines are similar at this point. However, both the moment and force stiffnesses are slightly higher for $l_f = 0.5L$ than for other set-ups. This was because this setup only used to the rear axle was used to brake, so the front tyres were less saturated. Therefore the standard deviation of the steering wheel velocity is slightly higher in figure 22a.

Apex ($s \approx 400\,\mathrm{m}$) There is little variation in the steering wheel velocity here with CoG position, and there is no difference in the controllability derivatives at the $l_f = 0.5L$ point. This is because the vehicle is not braking here, but has high lateral acceleration so all vehicles saturate their tyres equally and have equal derivatives. Hence the reduced braking performance of the $l_f = 0.5L$ vehicle has no effect.

Exit ($s \approx 480\,\mathrm{m}$) As previously stated, since the $l_f = 0.5L$ vehicle took a straighter line, it had a higher yaw rate on exit, and when the yaw stiffness was more negative, and hence the driver works hard at this point to control the disturbances, leading to the slight peak on exit, similar to that on entry. It slightly smaller as the velocity is lower on exit, so the lateral acceleration required and hence level of tyre saturation is smaller too, which means both controllability derivatives are higher.



(a) Standard deviation of steering wheel velocity (b) Moment steering "stiffness" (c) Force steering "stiffness"

Figure 22: Variation of controllability with centre of gravity position

Performance The performance of the vehicle greatly depends on the CoG position as shown in figure 23. The vehicle with the CoG in the middle is around 5% slower than the forward or rearward biased vehicles, which had an approximately similar performance. This is due to the reduced braking performance, since only the rear axle is used to brake, as previously mentioned.

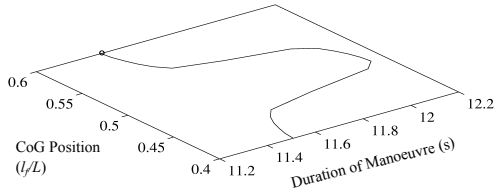


Figure 23: Variation of performance with centre of gravity position

7.5.3 Moment of Inertia

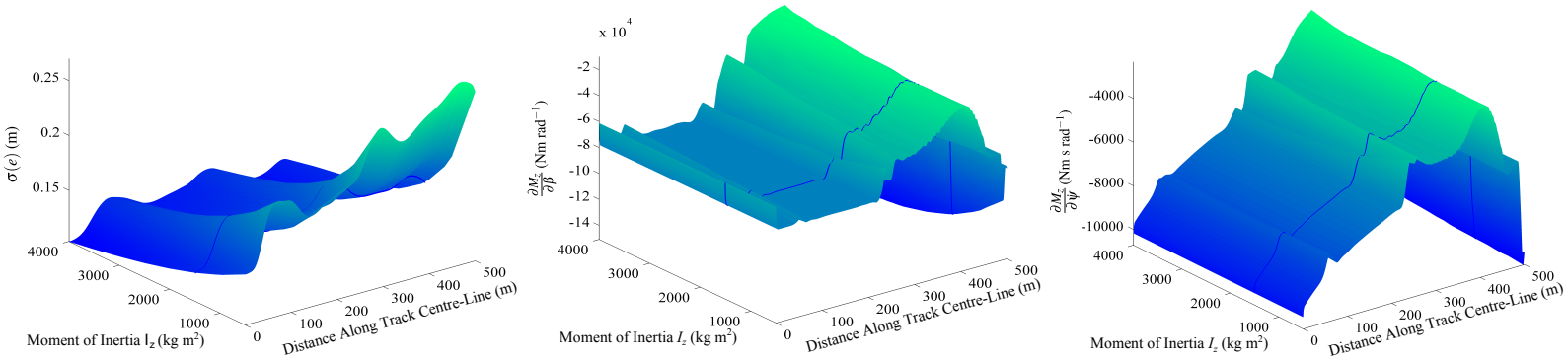
The yaw moment of inertia was altered around the nominal value of $1500\,\mathrm{kg\,m^2}$, ranging from $500\,\mathrm{kg\,m^2}$ up to $4000\,\mathrm{kg\,m^2}$. This was deemed to be a relevant parameter which is one an F1 team has control of. The results can be seem in figures 24, 25 and 26. It was found that, overall, reducing the moment of inertia compromises the stability, and also makes the driver work harder, in order to

control disturbances. There was very little effect on performance. However, since the reduction in stability makes the vehicle more maneuverable, there would be in reality a suitable compromise, but it was difficult to suggest which value this might be and would no doubt depend on the driver.

Stability

Approach ($s \lesssim 250\,\mathrm{m}$) As the yaw moment I_z is reduced, the standard deviation of the lateral path error increases. This is as expected, since if the yaw inertia is lower, but the force moment disturbances are the same, then this will result in larger accelerations, and hence attitude and path errors. However, this pattern is not directly reflected in the stability derivatives, since both the stiffness and damping metrics are independent of the yaw inertia. Despite this, the resulting decrease in stability could still have been inferred, if the damping coefficient and natural frequency were considered. These both increase with reducing moment of inertia, and hence the natural frequency will become closer to the excitation frequency, which will be high.

Entry ($s \approx 300\,\mathrm{m}$)**Apex** ($s \approx 400\,\mathrm{m}$) **& Exit** ($s \approx 480\,\mathrm{m}$) Similar trends are observed as during the approach phase. However, the effect is more noticeable at these points, as the yaw rates are higher.



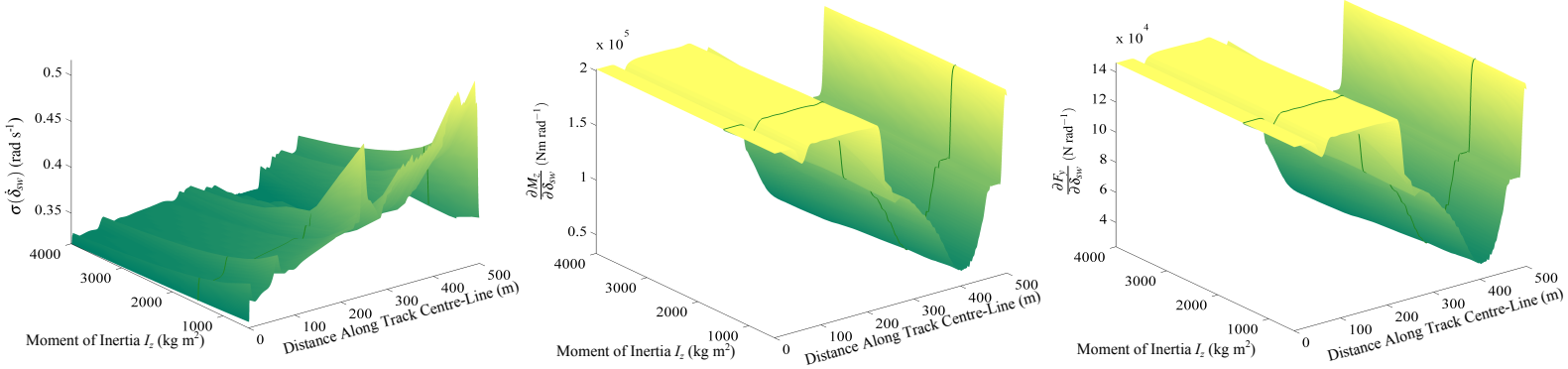
(a) Standard deviation of lateral path error (b) Yaw stiffness (c) Yaw damping

Figure 24: Variation of stability with yaw moment of inertia

Controllability

Approach ($s \lesssim 250\,\mathrm{m}$) Similar effects can be observed to the stability. The standard deviation of the steering wheel velocity in figure 22a increases slightly with reducing moment of inertia, because the driver must work harder to control the disturbances which propagate more readily as already explained. However, the the controllability derivatives in figures 22b and 22c show no difference, since they are independent of the moment of inertia, but of course, if the inertia is lower, the induced yaw moments from each steering wheel increment will have a larger effect.

Entry ($s \approx 300\,\text{m}$)**, Apex** ($s \approx 400\,\text{m}$) **& Exit** ($s \approx 480\,\text{m}$) Similar trends are observed as at approach. However, the increase in the steering wheel velocity with reducing moment of inertia is more noticeable at these points, as the low inertia vehicles are more unstable here. The controllability derivatives are still unaffected.



(a) Standard deviation of steering wheel velocity (b) Moment steering "stiffness" (c) Force steering "stiffness"

Figure 25: Variation of controllability with yaw moment of inertia

Performance It can be observed that the moment of inertia has a minimal effect on performance as shown in figure 23. Whilst the inertia affects the transient response of the vehicle, this has little effect over the longer timescale of the duration of the whole manoeuvre, because the driver can alter the nominal trajectory and controls, to take the increased delay into account.

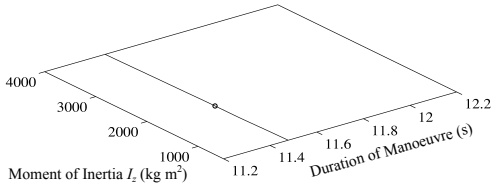


Figure 26: Variation of performance with yaw moment of inertia

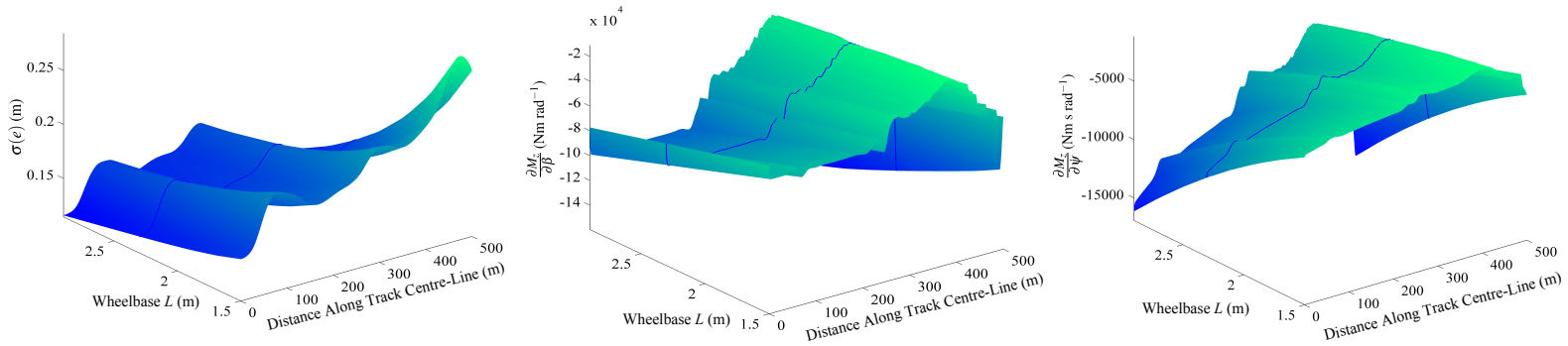
7.5.4 Wheelbase

Another parameter over which the teams have much control is the wheelbase. This was varied between 1.5 m and 2.9 m, and the results can be seen in figures 27, 28 and 29. It was found that the longer wheelbase improves both the stability and controllability without a significant reduction in performance, and thus it would be advantageous to choose as long a wheelbase as allowable with the rules.

Stability

Approach ($s \lesssim 250\,\text{m}$)**& Entry** ($s \approx 300\,\text{m}$) For these sections of the turn, the longer vehicles are more stable, since standard deviation of the lateral path error in figure 27a reduces. This can be explained by the increase in the yaw damping in figure 27c for the long vehicles, due to the longer tyre moment arms. This effect is larger than the reduction in the negative yaw stiffness in figure 27b, so overall, the longer vehicles are more stable.

Apex ($s \approx 400\,\mathrm{m}$) **& Exit** ($s \approx 480\,\mathrm{m}$) The stabilising effect of the longer vehicles is more marked here, because it is here when the yaw rate is high, so the longer wheelbase vehicles induce higher lateral slips in both tyres. This saturates the tyres more, so the steering disturbances from the driver propagate less. This appears to have been such that the spring stiffness does not change significantly with wheelbase, whilst there is still a noticeable difference in the yaw damping. This again suggests that it is here where the wheelbase has the greatest difference on the stability.



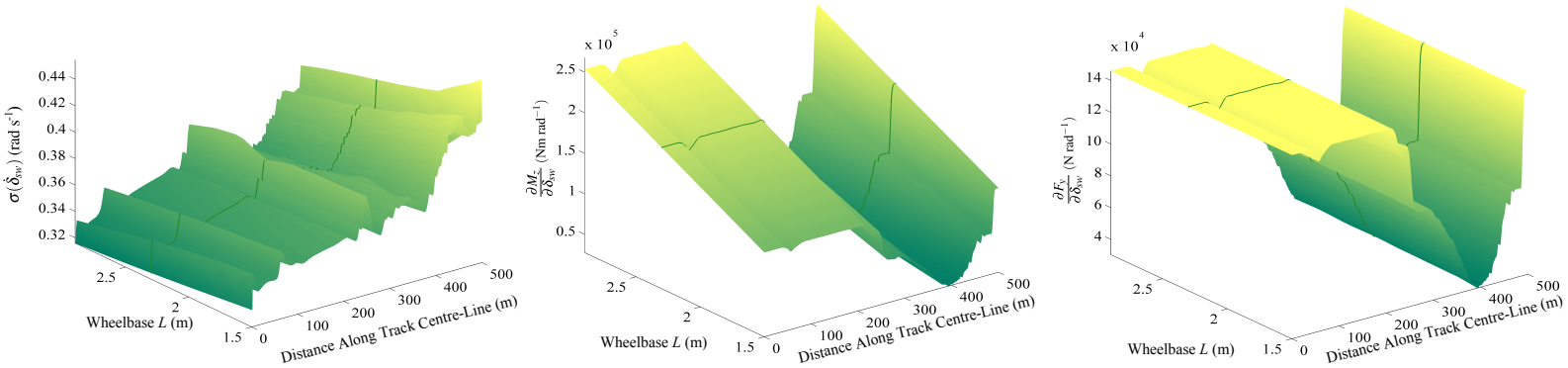
(a) Standard deviation of lateral path error (b) Yaw stiffness (c) Yaw damping

Figure 27: Variation of stability with wheelbase

Controllability

Approach ($s \lesssim 250\,\mathrm{m}$) **& Entry** ($s \approx 300\,\mathrm{m}$) The controllability exhibits similar trends to the stability. The standard deviation of the steering wheel rate in figure 28a does not vary significantly with wheelbase, before the turn suggesting the driver is working at his limit dictated by the LQR cost function. However, the moment stiffness controllability derivative in figure 28b is lower as the moment arms are reduced, suggesting more driver effort should be required; but this also means the steering disturbances propagate less, so it appears that the effects approximately cancel. The force "stiffness" controllability derivative in in figure 28c remains unaffected by the wheelbase as expected.

Apex ($s \approx 400\,\mathrm{m}$) **& Exit** ($s \approx 480\,\mathrm{m}$) The shorter vehicles require slightly more driver effort at these points according to the steering wheel velocity. However, the force steering "stiffness," although normally independent of wheelbase, this is in fact higher for the shorter wheelbase vehicles during the turn. Additionally, the moment "stiffness," normally linearly proportional to the wheelbase, becomes independent of wheelbase during the turn. These effects are because the larger vehicles saturate their tyres more here. However, since this means the steering disturbances propagate more, it appears the overall effect is that the driver effort must increase.



(a) Standard deviation of steering wheel velocity (b) Moment steering "stiffness" (c) Force steering "stiffness"

Figure 28: Variation of controllability with wheelbase

Performance The performance of the vehicle does not vary significantly with the wheelbase as shown in figure 29. This is because the transient performance does not vary, if the wheelbase is increased keeping moment of inertia fixed.

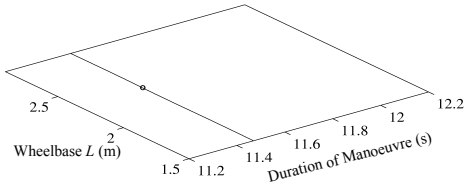


Figure 29: Variation of performance with wheelbase

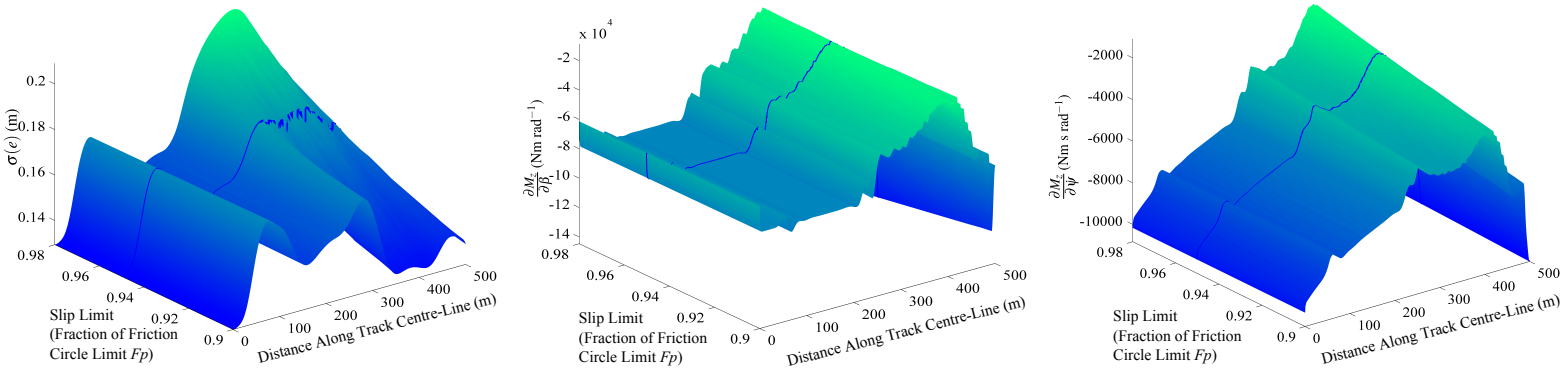
7.5.5 Tyre Slip Limit

When using Timings' MPC Lapsim tool, it was possible to put a constraint on the proportion of the friction circle radius F_p which the driver is to make use of. For the previous simulations, this was set at 0.95 so almost all of the force was utilised, but it was now varied around this value. The results can be seen in figures 30, 31 and 32. . It was found that increasing the slip limit shortens both the manoeuvre time as expected, but also compromises the handling performance, both in terms of controllability and stability. Therefore, there is clearly an optimum, which from these graphs, appeared to be around 0.96 for this vehicle and road geometry. This is intuitive, as it would be expected that the driver to drive as near to the limit as he can control the vehicle, but other factors such as tyre wear will impose limitations.

Stability

Approach ($s \lesssim 250\,\mathrm{m}$) From the lateral path error standard deviation in figure 30a, as well as the stability derivatives, that there is no effect up until entry into the turn. This is because the accelerations, and hence forces and tyre slips are lower here, and not near the friction limit.

Entry ($s \approx 300\,\mathrm{m}$)**, Apex** ($s \approx 400\,\mathrm{m}$) **& Exit** ($s \approx 480\,\mathrm{m}$) On entry, and even more so on exit, the higher the slip limit, the much less stable the vehicle is, since for this part of the manoeuvre, the tyres are nearest to the friction circle, so the slip limit has an effect. If more of the friction circle is used, the effective stiffness of the tyres reduces, so the yaw stiffness is slightly less negative during the turn, stabilising the vehicle, as shown in in figure 30b. The yaw damping in figure 30c, however, depends both on forward velocity as well from (5.1.2). The vehicle can remain at a higher velocity for the higher slips, and therefore the yaw damping reduces significantly for the higher slips. Hence, overall, the higher the slip limit, the less stable the vehicle is.



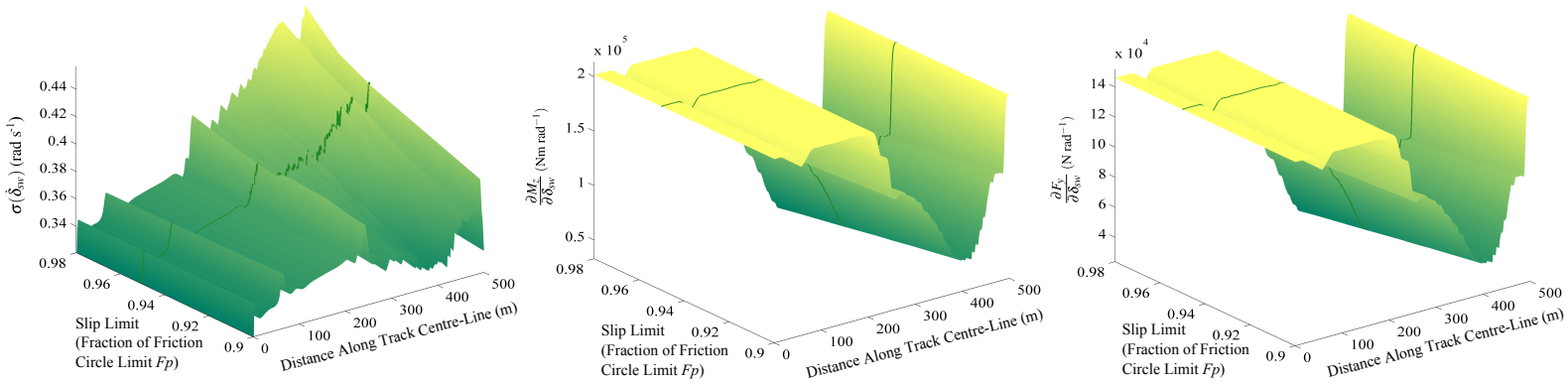
(a) Standard deviation of lateral path error (b) Yaw stiffness (c) Yaw damping

Figure 30: Variation of stability with tyre slip limit

Controllability

Approach ($s \lesssim 250\,\mathrm{m}$) The controllability is affected in a similar manner to the controllability. On approach, there is little variation, as the slips are not near the friction circle.

Entry ($s \approx 300\,\mathrm{m}$)**, Apex** ($s \approx 400\,\mathrm{m}$) **& Exit** ($s \approx 480\,\mathrm{m}$) During the turn, the standard deviation of the steering wheel velocity in figure 31a is significantly higher for the higher slip limits. This is because the tyres are more saturated, so larger steering angles are required to generate large enough forces to attenuate these disturbances, as reflected in both the force and moment stiffness controllability derivatives in figures 30b and c, which are lower during the turn for the higher slips. This is partly beneficial, as it means that the effect of the steering disturbances is reduced.



(a) Standard deviation of steering wheel velocity (b) Moment steering "stiffness" (c) Force steering "stiffness"

Figure 31: Variation of controllability with tyre slip limit

Performance This parameter has the greatest effect on the vehicle performance, with higher slips leading to reduced manoeuvre times, as expected. If more of the friction circle is utilised, the vehicle can accelerate faster longitudinally, as well as laterally, so can take the corner at a greater speed.

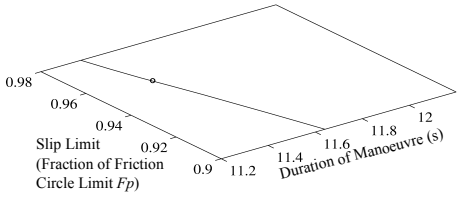


Figure 32: Variation of stability, controllability and performance with tyre slip limit

8 Conclusions

It is clear from the work completed in this project that the two different methods for characterising the stability and controllability, each have their own relative advantages and disadvantages, but potentially have far reaching applications if further refined. Firstly, it was demonstrated that the problems with the state variance stability metrics from the previous work from Sideris [1], could indeed be fixed with the introduction of a Linear-Quadratic Controller, which allowed the steady-state error in the lateral path and attitude errors to be removed because of the closed loop control. The yaw stability derivatives were also successfully implemented, but these were found to be difficult to interpret, because of the interaction of both terms, and that the yaw stiffness can often be negative. On the other hand, the standard deviation based methods were much easier to interpret, as one value, such as the standard deviation of the lateral path error, can be given, with an obvious physical interpretation, accounting for the closed-loop control from the driver.

It was shown to be possible to extend each of these derivatives to assess the controllability also. Using the state variance matrix, the variances of the driver controls were found, and controllability derivatives from the literature, were also implemented. Since the LQR controller was chosen to only introduce steering terms to stabilise the vehicle, and the controllability derivatives specified the

steering "stiffness", only the steering effort was characterised. The standard deviation of the steering wheel velocity was used, since this was deemed to be a better measure of the driver effort. As with the stability, the standard deviations were found to be much more simple to interpret, and a better measure of driver effort. This is because they account for the fact that the vehicle may be inherently less stable, thus leading to more driver work to control the vehicle, whereas the derivatives only quantify the effect of each steering wheel increment.

The nominal control inputs required to allow the vehicle to navigate along an optimal trajectory around a 90° bend were found using the work of Timings [9], which then facilitated a parameter study. The effect of each parameter could be evaluated on handling using the developed metrics, and suitable optimal values for each were suggested, as follows:

- **Brake Balance:** Rear-biased vehicle tended to be less stable and controllable on entry, whilst front-biased vehicle tended to be less so on exit, so there was an optimum around $b_f \approx 0.4$, which spread the braking forces more evenly. This also lead to an improved braking performance, and hence a shorter manoeuvre time.

- **Centre of Gravity Position:** The forward biased vehicles were generally more stable, but the rearward biased vehicles were more controllable, with little change in the performance. Therefore it was concluded that a rearward biased setup would most likely be deemed more desirable, as this improvement in controllability makes the vehicle more manoeuvrable, also avoiding the issues of instability associated with oversteering vehicles.

- **Yaw Moment Of Inertia:** Increasing the moment of inertia made the vehicle more stable and controllable, without a significant drop in performance, except for centrally placed CoG's which were far slower. However, since making the vehicle less stable does make the vehicle more manoeuvrable, so there would be a trade-off in reality.

- **Wheelbase:** Longer vehicles were found to be both more stable and controllable, without compromising performance, and so as long a wheelbase as is allowable with the rules should be chosen.

- **Tyre Slip Limit:** The more of the friction circle is made use off, the less stable and controllable the vehicle becomes, but there is a large reduction in manoeuvre time. Therefore the driver would wish to drive as close to the full slip limit as he can manage, although tyre wear considerations would also play a crucial role.

As well as providing insight into the mechanics of the vehicle, the parameter study allowed the stability and controllability metrics to be assessed further. It was found that, as before, the standard deviation based metrics were much easier to interpret, but they provide little indication as to what

has caused the change in handling behaviour. This was where the derivative based methods were superior.

In terms of computational efficiency, for the simple 5DOF model in this study, both metrics took very little CPU time to compute, and were far more efficient than the alternative methods discussed in section 2. A full 650 iteration manoeuvre lasting 13 s in real-time could be computed in around 26 s, but this included much lead time, and could no doubt be improved. Therefore it is possible that these metrics could be computed in real-time on a simulator. For more complex vehicle models with more degrees of freedom, the variance-based metric computation time is likely to increase because the covariance matrices will increase in size; whereas the derivatives may be less sensitive to this, as these only require the tyre slips and simple differentiation. However, this was not investigated in this work.

Overall, it was concluded that, in order to characterise the stability and controllability, the standard deviation based methods were the superior metrics, as they could generate one simple quantity, so were far easier to interpret. They could therefore be of great use perhaps when communicating to the driver, or could be fed back into optimal path tools such as the one used in this work [9], so the racing line could account for the handling performance. However, in order to help guide potential set-up changes, the derivatives are very effective supplementary metrics since they provide greater insight into the mechanics of the vehicle.

9 Future Work

This work built upon and extended the ideas from Sideris [1], but there is definite scope for further improvement and refinement. More work could go in developing further understanding of how the derivatives and variances together represent the stability and controllability, and perhaps some of the other derivatives and standard deviations not looked at in this work may be of interest. The parameter study in this work was not very comprehensive and further insight could be gained in this area, particularly when multiple variables are changed, as many will in fact be interlinked. Additionally, different types of manoeuvre and whole laps should be investigated, to gain a fuller picture of the overall effect of each parameter.

The vehicle model could be made more sophisticated, by including in aerodynamic and engine maps, which play a very important role in the transient response of F1 cars. However, perhaps more important than the vehicle model is the driver model, as this is what ultimately determines how stable the vehicle is, particularly when approaching the limit. The driver model used in the project was very simple, but would need to be refined if were to be used for practical simulations. There are various cognitive delays and bandwidths which were not taken into account. There may also be a discrepancy between the vehicle model the driver attempts to the control, and the one in his mind, as he does not have full information. This work only looked at lateral stability, but if a realistic speed control model was used, then this would allow the longitudinal stability to also be assessed.

Computational complexity and other practical issues need to be considered further. Although for the simple vehicle model in this project, the methodology was found to be very computationally efficient, it has yet to be seen how this would increase with the number of degrees of freedom, the refresh rate and so on. The variance methods required a state-space model, but in practice, the dynamics are likely to be presented in a non-linear symbolic form. This model could be symbolically linearised to make use of the existing method used in this work, but this may present its own computational challenges.

Risk Assessment Retrospective

In the risk assessment submitted prior to the commencement of the project during the Michaelmas term in 2011, the only risks identified were associated with the high levels of computer usage required. Numerous hours were spent on a notebook computer, which is not particularly ergonomic, in order to write the code, run simulations, as well as review the outputs, which is a highly cognitive and dextrous task. The main problems that can therefore arise are repetitive strain injuries in the fingers, and back and eye strain from a poor seating position and viewing angle. These problems were anticipated on the assessment form, and were avoided with the use of an external keyboard and an adjustable desk chair. Additionally, regular breaks were taken, and it was ensured that the room was well lit to further reduce the risk of eye strain.

References

[1] M. Sideris. F1 car stability analysis. Master's thesis, Department of Engineering, University of Cambridge, 2011.

[2] V. Nguyen. Vehicle handling, stability and bifurcation analysis for nonlinear vehicle models. Master's thesis, Faculty of the Graduate School of the University of Maryland, 2005.

[3] H. B. Pacjeka. Simplified analysis of steady-state turning behaviour of motor vehicles. part 1. handling diagrams of simple systems. *Vehicle System Dynamics*, 2(3):161–172, 1973.

[4] W. Milliken and D. Milliken. *Race Car Vehicle Dynamics*. Society of Automotive Engineers, 1995.

[5] H. J. Kohn. *Controllability of Road Vehicles at the Limits of Tyre Adhesion*. PhD thesis, School of Mechanical Engineeirng, Cranfield University, 1998.

[6] H. H. Rosenbrook. The stability of linear time-dependent control systems. *Journal of Electronics and Control*, 15(1):73–80, 1963.

[7] Hurwitz A. On the conditions under which an equation has only roots with negative real parts, 1964.

[8] J. Meijaard and A. Popov. Practical stability analysis for transient system dynamics. *Proceedings of the Institution of Mechanical Engineers, Part C: Journal of Mechanical Engineering Science*, 222(11):2123–2135, 2008.

[9] J. Timings. *Application of Convex Optimisation and Robust Control to Dynamic Lap-Time Simulation*. PhD thesis, Department of Engineering, University of Cambridge, 2012.

[10] D. J. Cole, A. J. Pick, and A. M. C. Odhams. Predictive and linear quadratic methods for potential application to modelling driver steering control. *Vehicle System Dynamics*, 44(3):259–284, 2006.

[11] M. C. Best and T. J. Gordon. On the synthesis of driver inputs for the simulation of closed-loop handling manoeuvres. *International Journal of Vehicle Design*, 40(1–3):52–76, 2006.

[12] H. B. Pacejka. *Tyre and Vehicle Dynamics*. Butterworth Heineman, Oxford, 2002.

[13] A. Pick and D. Cole. Neuromuscular dynamics and the vehicle steering task. *Vehicle System Dynamics*, 41:182–191, 2005.

[14] J.P. Timings and D.J. Cole. Efficient minimum manoeuvre time optimisation of an oversteering vehicle at constant forward speed. pages 5267–5272. American Control Conference (ACC), June 2011.

[15] Ulsoy A.G. Lin, C. and D.J. LeBlanc. Vehicle dynamics and external disturbance estimation for vehicle path prediction. *Control Systems Technology, IEEE Transactions on*, 8(3):508 –518, May 2000.

[16] M. Shahian B., Hassul. *Control system design using MATLAB*. Prentice Hall, NJ, 1993.

[17] K. Åström and K. Johan. *Feedback systems: an introduction for scientists and engineers*. Princeton University Press, NJ, 2008.

[18] Mohamed M. ElMadany and Zuhair S. Abduljabbar. Linear quadratic gaussian control of a quarter-car suspension. *Vehicle System Dynamics*, 32(6):479–497, 1999.

[19] Powell J.D. Franklin, G. F. and A. Emami-Naeini. *Feedback Control of Dynamic Systems*. Prentice Hall, NJ, fourth edition, 2002.

[20] M. Grewal and A.P. Andrews. *Kalman Filtering: Theory and Practice Using MATLAB*. Wiley & Sons, NY, 2001.

[21] M. Apetaur and F. Opička. Assessment of the driver's effort in typical driving manoeuvres for different vehicle configurations and managments. *Vehicle System Dynamics: International Journal of Vehicle Mechanics and Mobility*, 20(suppl. 1):42–56, 1992.